

Pyrochlore Photons: The $U(1)$ Spin Liquid in a $S = 1/2$ Three-Dimensional Frustrated Magnet

Michael Hermele,¹ Matthew P. A. Fisher,² and Leon Balents¹

¹*Department of Physics, University of California, Santa Barbara, CA 93106-9530*

²*Kavli Institute for Theoretical Physics, University of California, Santa Barbara, CA 93106-4030*

(Dated: January 28, 2020)

We study the $S = 1/2$ Heisenberg antiferromagnet on the pyrochlore lattice in the limit of strong easy-axis exchange anisotropy. We find, using only standard techniques of degenerate perturbation theory, that the model has a $U(1)$ gauge symmetry generated by certain local rotations about the z -axis in spin space. Upon addition of an extra local interaction in this and a related model with spins on a three-dimensional network of corner-sharing octahedra, we can write down the exact ground state wavefunction with no further approximations. Using the properties of the soluble point we show that these models enter the $U(1)$ spin liquid phase, a novel fractionalized spin liquid with an emergent $U(1)$ gauge structure. This phase supports gapped $S^z = 1/2$ spinons carrying the $U(1)$ “electric” gauge charge, a gapped topological point defect or “magnetic” monopole, and a gapless “photon,” which in spin language is a gapless, linearly dispersing $S^z = 0$ collective mode. There are power-law spin correlations with a nontrivial angular dependence, as well as novel $U(1)$ topological order. This state is stable to *all* perturbations and exists over a finite extent of the phase diagram. Using a convenient lattice version of electric-magnetic duality, we develop the effective description of the $U(1)$ spin liquid and the adjacent soluble point in terms of Gaussian quantum electrodynamics and calculate a few of the universal properties. The resulting picture is confirmed by our numerical analysis of the soluble point wavefunction. Finally, we briefly discuss the prospects for understanding this physics in a wider range of models and for making contact with experiments.

I. INTRODUCTION

The search for quantum spin liquid states in frustrated magnets can be traced back at least as far as the early suggestion of a resonating valence bond state in the triangular lattice Heisenberg model¹. Almost 15 years later, the suggestion of such a state in the undoped high- T_c cuprates² set off an explosion of interest in two-dimensional spin liquids (i.e. Mott insulators at half-filling with *no* broken symmetries). Frustrated Heisenberg models on the square, triangular and kagomé lattices have all received significant attention as candidate systems for quantum disordered ground states. While there has been comparatively little theoretical work on quantum spin liquids in three-dimensional frustrated magnets, materials with magnetic ions on the pyrochlore lattice (Fig. 2) may be good candidates for spin liquids and other exotic states. To give one example, recent neutron scattering experiments on ZnCr_2O_4 , a $S = 3/2$ pyrochlore Heisenberg antiferromagnet, suggest a nontrivial disordered state³ above a transition to Néel order accompanied by a lattice distortion⁴ at 12.5 K.

Meanwhile, much work has been devoted to understanding the properties of possible spin liquid states, independent of their existence in particular microscopic models. Most of the proposed spin liquid states support deconfined $S = 1/2$ spinons; such states are fractionalized in that some of the elementary excitations carry quantum numbers that are fractions of those allowed in a finite-size system. Fractionalized states can be precisely characterized by their *topological order*⁵, which in the simplest scenario is associated with the topological sectors of an emergent, deconfining Z_2 gauge field⁶. The

“vison,” a gapped vortex-like excitation that carries the Z_2 flux, must also be present. While topological order does not require a liquid ground state and can coexist with conventional long-range order, we believe it is probably common in spin liquids and hence in some of the nearby ordered states. Very recently, many of these ideas have been put on firmer ground by the emergence of several microscopic models supporting stable fractionalized phases in two and three dimensions^{7,8,9,10,11,12}.

Despite these recent theoretical successes, an unambiguous experimental realization of these ideas is still lacking. Indeed, spin liquid states seem rather rare; is topological order rare as well? For Z_2 -fractionalized states this question is difficult to answer, because the gapped visons have no effect on easily measurable low-energy properties. Clever proposals have been made¹³ and carried out^{14,15} to directly detect topological order in the cuprates (with negative results thus far), but these experiments are difficult and rely on properties of the phases proximate to a topologically ordered state. Z_2 topological order is difficult enough to observe that it is impossible to say at present how rare or common it is.

Fortunately it may be possible to shed new light on the experimental situation. In this paper, we present two models of *three-dimensional* $S = 1/2$ frustrated magnets, one on the pyrochlore lattice, the other on a related network of corner-sharing octahedra (the links of the cubic lattice, as shown in Fig. 5). Both of these models exhibit a novel fractionalized phase, the $U(1)$ spin liquid. This state has an emergent $U(1)$ gauge structure that gives rise to several remarkable properties: there is a *gapless* “artificial photon” excitation, a gapped spinon carrying “electric” gauge charge, a gapped spinon carrying “magnetic” monopole,

an emergent $1/r$ “Coulomb” potential between pairs of spinons and monopoles, and novel $U(1)$ topological order. If this phase exists in a real material, the gapless photon should have important implications for low-energy thermodynamics, transport and spectroscopy; therefore $U(1)$ fractionalization may be easier to find in experiments. Such states, thus far realized in large- N spin models¹⁶ and bosonic Hubbard-type models^{9,10,11}, arise as the deconfined or Coulomb phase of compact $U(1)$ lattice gauge theory. While most work on spin liquids has focused on $d \leq 2$, motivated by the cuprates and the conventional wisdom that quantum fluctuations are more effective at destroying long range order in low dimensions, the $U(1)$ spin liquid *only* occurs in $d \geq 3$; for $d \leq 2$ the Coulomb phase of compact $U(1)$ gauge theory is always unstable due to instanton effects¹⁷.

Both models are of intrinsic interest as examples of tractable but nontrivial frustrated magnets. The pyrochlore model is particularly appealing due to its simplicity: its derivation begins with the nearest-neighbor $S = 1/2$ Heisenberg antiferromagnet. Taking the limit of large easy-axis exchange anisotropy $J_z \gg J_{\perp}$ simplifies the problem by breaking the spectrum into extensively degenerate manifolds with large separations of $O(J_z)$. It is then possible to write an effective Hamiltonian describing the splitting of the low-energy manifold, using standard techniques of degenerate perturbation theory in J_{\perp} . This effective Hamiltonian *has* a $U(1)$ gauge structure, which forms the foundation for our subsequent analysis¹⁸. Another point of view, equivalent at the level of perturbation theory but perhaps with broader implications in more general scenarios, is that the low-energy sector of the model is *unitarily equivalent* to a $U(1)$ gauge theory. It is not obvious how to treat the resulting model analytically, but upon addition of an extra six-site interaction term it can be tuned to a soluble point where it is possible to write an exact ground state wavefunction with no further approximations. The models can be reinterpreted as quantum dimer models (QDMs), and the extra term as the analog of the Rokhsar-Kivelson (RK) potential in the square lattice QDM¹⁹. As will be explained in detail below, the properties of the soluble point allow us to locate the $U(1)$ spin liquid adjacent to it. Since this state is stable to *all* perturbations, it persists over a finite extent of the phase diagram (Fig. 1). Furthermore, stability to large but finite J_z implies that the $U(1)$ gauge structure persists in the absence of microscopic local symmetries and is truly emergent. On the purely theoretical side, we believe these models give the first examples of $U(1)$ gauge theories that have a deconfining phase even in the limit of infinitely strong bare coupling. The first such Z_2 gauge theory was discovered only recently by Moessner and Sondhi⁷.

The effective theory of the $U(1)$ spin liquid and the soluble RK point is simply Gaussian quantum electrodynamics (QED). At the RK point, which is itself a special deconfined limit of the generic phase, the “electric stiffness,” or coefficient of \mathbf{E}^2 in the Hamiltonian, van-

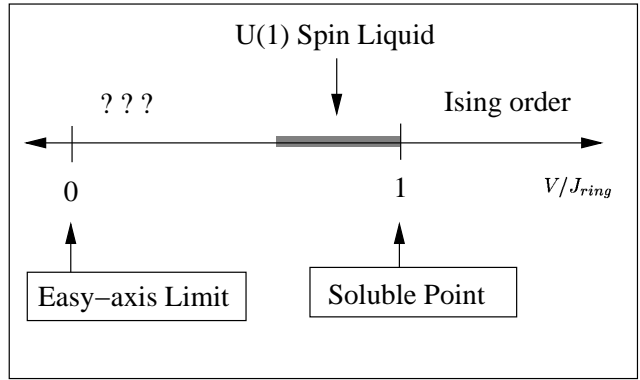


FIG. 1: Phase diagram for both models. The parameter V/J_{ring} is the relative strength of the Rokhsar-Kivelson potential and the XY ring exchange that obtains in the easy-axis limit of the Heisenberg model. The soluble point is located at $V/J_{ring} = 1$, which is a special deconfined point of the adjacent $U(1)$ spin liquid. Just to the right of the soluble point the models go into an Ising ordered state. Sufficiently far to the left we expect Ising-ordered and/or plaquette density wave states with broken translation symmetry but no magnetic order. Immediately to the left of the soluble point, the $U(1)$ spin liquid exists over a finite (but unknown) extent of the phase diagram.

ishes. This is a higher-dimensional generalization of the effective picture of the square lattice QDM in terms of a coarse-grained height field²⁰.

The $U(1)$ spin liquid has power-law correlations with nontrivial angular dependence, novel $U(1)$ topological order, and supports gapped $S^z = 1/2$ spinons, a gapped topological point defect (the “magnetic” monopole) and a gapless $S^z = 0$ collective mode corresponding to the photon of the gauge theory. The latter excitation makes an additive T^3 contribution to the low-temperature specific heat, and should affect various other low-energy properties of $U(1)$ -fractionalized phases (either the $U(1)$ spin liquid, or phases with coexisting conventional and topological order). If such a phase exists in a real material, we speculate that it may be possible to probe “photons” with photons via Raman scattering.

A. Outline

We begin Sec. II with a derivation of the pyrochlore model starting from the Heisenberg antiferromagnet. In Sec. II B the cubic (or corner-sharing octahedra) model is discussed. The remainder of Sec. II is concerned with demonstrating the equivalence of the spin models to frustrated compact $U(1)$ gauge theories, and developing a useful lattice version of electric-magnetic duality.

Beginning from the dual description, Sec. III develops the effective description of the $U(1)$ spin liquid and the soluble point in terms of Gaussian quantum electrodynamics.

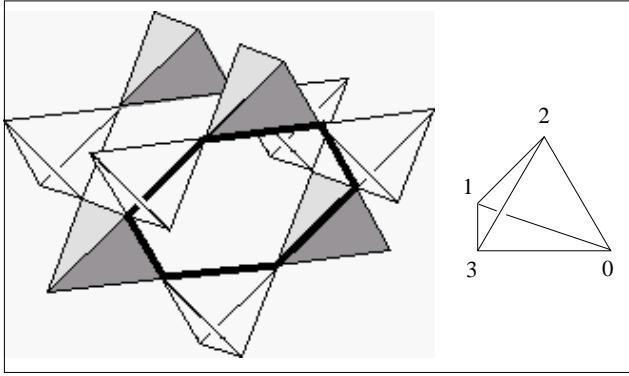


FIG. 2: The pyrochlore lattice (left), and one up-pointing tetrahedron (right). One sublattice of tetrahedra is shaded, and the other transparent. The thickened bonds show the location of a pyrochlore hexagon. Each such hexagon is a member of one of four orientations of kagomé lattice planes. The numbering of sites in the up-pointing tetrahedron on the right is the convention used in the text. For $i = 0, 1, 2$, the fcc Bravais lattice vector \mathbf{a}_i points in the direction given by looking from site 3 to site i .

namics. Corrections to effective action and to the scaling equalities between microscopic and effective degrees of freedom are discussed in Sec. III C. Sec. IV contains a discussion of the universal properties of the $U(1)$ spin liquid, including its novel $U(1)$ topological order. In Sec. V we present our analysis of the soluble point ground state wavefunction, which gives strong support for the validity of our effective picture. We conclude in Sec. VI with a discussion of open issues, focusing on the challenging problems of understanding this physics in a broader range of models and looking for $U(1)$ -fractionalized phases in real materials.

II. MODELS AND MAPPINGS

A. Pyrochlore Model

We begin with the nearest-neighbor $S = 1/2$ Heisenberg antiferromagnet on the pyrochlore lattice. This structure is a three-dimensional network of corner-sharing tetrahedra (Fig. 2). It can be obtained by translating one “up-pointing” tetrahedron (shown on the right of Fig. 2) through the fcc Bravais lattice vectors $\mathbf{R} = n_0 \mathbf{a}_0 + n_1 \mathbf{a}_1 + n_2 \mathbf{a}_2$. We choose $\mathbf{a}_0 = \mathbf{x}$, $\mathbf{a}_1 = \mathbf{x}/2 + \sqrt{3}\mathbf{y}/2$, and $\mathbf{a}_2 = \mathbf{x}/2 + \mathbf{y}/2\sqrt{3} + \sqrt{2/3}\mathbf{z}$. Basis vectors for the reciprocal lattice are defined by $\mathbf{b}_i = \sqrt{2}\pi\epsilon_{ijk}\mathbf{a}_j \times \mathbf{a}_k$, so that $\mathbf{a}_i \cdot \mathbf{b}_j = 2\pi\delta_{ij}$. The four sites in each unit cell are distinguished by an index $i = 0, \dots, 3$, as indicated in Fig. 2. Up to a constant the Hamiltonian can be written

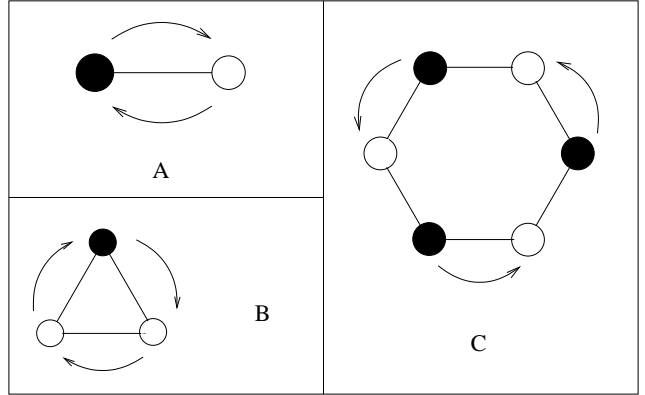


FIG. 3: Depiction of the processes contributing to the third-order degenerate perturbation theory for the easy-axis pyrochlore Heisenberg antiferromagnet. Processes (A) and (B) give only trivial constant shifts of the energy. Process (C) leads to an XY ring exchange term acting on hexagonal plaquettes.

as a sum over tetrahedra:

$$\mathcal{H} = \frac{J}{2} \sum_t (\mathbf{S}_t)^2, \quad (1)$$

where $\mathbf{S}_t = \sum_{i \in t} \mathbf{S}_i$ is the total spin on the tetrahedron t . Following the analysis of a generalized kagomé Heisenberg antiferromagnet in Ref. [8], we introduce easy-axis exchange anisotropy:

$$\mathcal{H} = \mathcal{H}_I + \mathcal{H}', \quad (2)$$

$$\mathcal{H}_I = \frac{J_z}{2} \sum_t (S_t^z)^2, \quad (3)$$

$$\mathcal{H}' = \frac{J_\perp}{2} \sum_{\langle ij \rangle} (S_i^+ S_j^- + h.c.), \quad (4)$$

where $J_z \gg J_\perp$. This reduces the global $SU(2)$ invariance to $U(1) \times Z_2$. We first consider the point $J_\perp = 0$, where \mathcal{H} reduces to a classical Ising model, with ground states specified by $S_t^z = 0$ on all tetrahedra. It was argued by Anderson²¹ that, almost identically to Pauling’s model for water ice²², this Ising model has an extensive ground state degeneracy (i.e. finite $T = 0$ entropy per site).

A small $J_\perp > 0$ introduces quantum fluctuations and lifts the extensive degeneracy; this splitting is encapsulated in an effective Hamiltonian using standard techniques of perturbation theory. The first-order contribution is easily seen to vanish. We will need to go to third order, where we have the general expression:

$$\mathcal{H}_{eff} = (1 - \mathcal{P}) \left[-\mathcal{H}' \frac{\mathcal{P}}{\mathcal{H}_I} \mathcal{H}' + \mathcal{H}' \frac{\mathcal{P}}{\mathcal{H}_I} \mathcal{H}' \frac{\mathcal{P}}{\mathcal{H}_I} \mathcal{H}' \right] (1 - \mathcal{P}). \quad (5)$$

Here \mathcal{P} projects onto the orthogonal complement of the ground state manifold. To describe the processes contributing in Eq. (5), it is useful to work in the standard

hardcore boson language for the spins, where $S^z = \pm 1/2$ corresponds to the presence/absence of a boson. Each term in \mathcal{H}' hops bosons along nearest-neighbor bonds; acting on a state in the low-energy manifold, each hop creates two tetrahedra with $S_t^z \neq 0$. At second order in \mathcal{H}' , bosons can hop and then return along the same bond (Fig. 3A). This can always occur on 4 bonds in every tetrahedron, thus giving only a constant contribution to the energy. At third order another constant contribution arises from single bosons (or holes) hopping around triangular faces (Fig. 3B). There is also a nontrivial *ring exchange* process acting on the hexagonal plaquettes (see Fig. 2), where hexagons containing three evenly spaced bosons can be rotated as shown in Figure 3C. The resulting effective Hamiltonian is

$$\begin{aligned} \mathcal{H}_{eff} = & (J_\perp^2/J_z)(J_\perp/J_z - 1)N_t & (6) \\ & + J_{ring} \sum_{\bigcirc} (S_1^+ S_2^- S_3^+ S_4^- S_5^+ S_6^- + h.c.), \end{aligned}$$

where N_t is the total number of tetrahedra, $J_{ring} = 3J_\perp^3/2J_z^2$, and the sum is over hexagonal plaquettes. The labelling of the spin operators inside the sum is given by moving around each hexagon in an arbitrary direction. Note that $[\mathcal{H}_{eff}, S_t^z] = 0$, as must be true for *any* effective Hamiltonian acting in the low-energy manifold, whatever the form of \mathcal{H}' .

It is possible, and will be convenient, to change the sign of the ring term by a similarity transformation. On any given site we can make the transformation $S^z \rightarrow S^z$ and $S^\pm \rightarrow -S^\pm$ by making a π -rotation about the z -axis in spin space. One transformation with the desired effect, consisting of π -rotations on a pattern of sites, is:

$$S_i^z \rightarrow S_i^z \quad (7)$$

$$S_{\mathbf{R}i}^\pm \rightarrow \exp(i\mathbf{Q}_i \cdot \mathbf{R})S_{\mathbf{R}i}^\pm, \quad (8)$$

where $\mathbf{Q}_{0,1} = (\mathbf{b}_1 + \mathbf{b}_2)/2$ and $\mathbf{Q}_{2,3} = 0$.

After this transformation the Hamiltonian takes the form

$$\mathcal{H}_p = -J_{ring} \sum_{\bigcirc} (S_1^+ S_2^- S_3^+ S_4^- S_5^+ S_6^- + h.c.), \quad (9)$$

where the constant terms have been dropped. Models similar to this one on the kagomé⁸, square²³ and triangular²⁴ lattices, where XY ring exchange of spins or bosons is a dominant term, have recently been shown to exhibit a variety of unusual phases and critical behavior. The physics of the pyrochlore ring exchange model should be accessible to quantum Monte Carlo studies; while the original Hamiltonian in Eq. (2) has a sign problem, \mathcal{H}_p does not.

\mathcal{H}_p can be reinterpreted as a quantum dimer model on the diamond lattice (Fig. 4), with two dimers touching every site. To see this, observe that the centers of the pyrochlore tetrahedra form a diamond lattice. Each nearest-neighbor diamond link passes through exactly one pyrochlore site, so we can reinterpret the pyrochlore

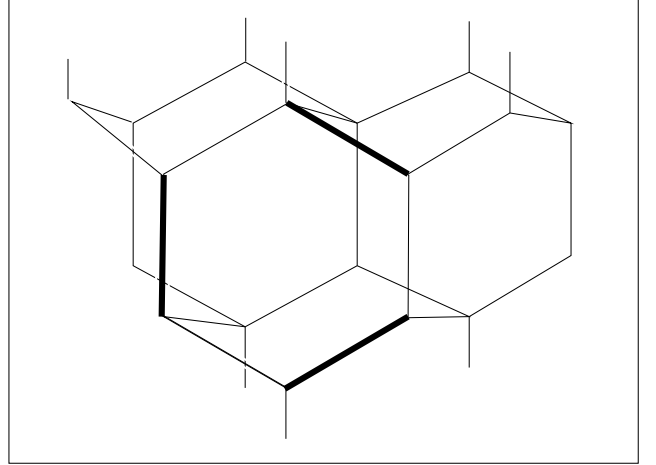


FIG. 4: A small piece of the diamond lattice. The links form hexagonal loops corresponding to the pyrochlore hexagons. These are the shortest possible closed paths on the diamond lattice. The hexagon with three thickened bonds depicts the dimer positions on a flippable hexagon. The alternating full and empty bonds correspond to alternating up and down spins.

spins as diamond link variables. The smallest closed loops in this lattice contain six links and correspond to the pyrochlore hexagons. We say a dimer is present on a given bond if $S_i^z = 1/2$, or absent if $S_i^z = -1/2$. $S_t^z = 0$ becomes the constraint that every diamond *site* touches two dimers, and the ring exchange move is the most local dynamics preserving this constraint. Each term in \mathcal{H}_p acts on a ‘flippable’ hexagon, one containing alternating full and empty bonds as in Fig. 4, by rotating the dimers around it. Non-flippable hexagons are annihilated.

As first realized by Rokhsar and Kivelson, dimer models generically have a point in their parameter space where it is possible to write down the exact ground state wavefunction¹⁹. To reach this point in our model, we add the term $\mathcal{H}_V = VN_f$, where N_f is the number of flippable hexagons. The RK point obtains for $\mathcal{H}_{RK} = \mathcal{H}_p + J_{ring}N_f$ (i.e. $V = J_{ring}$), and the ground state is an equal-weight superposition of all possible dimer coverings of the lattice that satisfy the constraint of two dimers touching every site. In the spin language, this wavefunction can be written as the projection of a transverse ferromagnet:

$$|\psi_{RK}\rangle = (1 - \mathcal{P}) \prod_i |\mathcal{S}_i^x = 1/2\rangle, \quad (10)$$

where, as in Eq. (5), $(1 - \mathcal{P})$ projects onto the $S_t^z = 0$ manifold. For completeness, we also express N_f in terms of spin operators: $N_f = \sum_{\bigcirc} P_{flip}(\bigcirc)$, where $P_{flip}(\bigcirc)$ gives unity acting on a flippable hexagon and zero other-

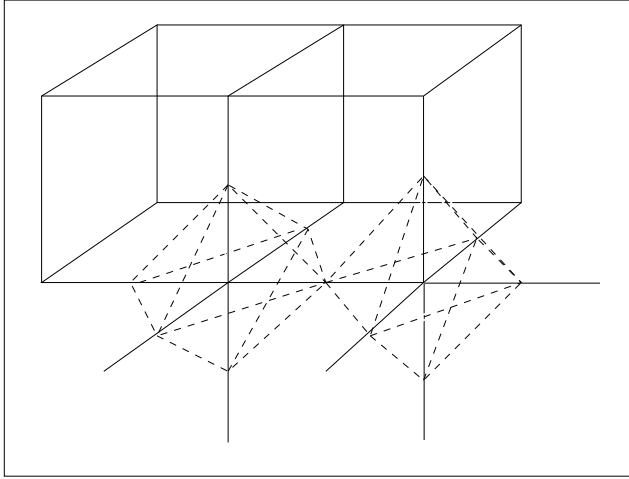


FIG. 5: Illustration that the *links* of the cubic lattice are equivalent to the *sites* of a lattice of corner-sharing octahedra.

wise. One has:

$$P_{flip}(\mathcal{O}) = \sum_{\sigma=\pm 1} \prod_{j \in \mathcal{O}} \left(\frac{1}{2} + \sigma(-1)^j S_j^z \right). \quad (11)$$

We will be interested in the properties of the generalized ring model $\mathcal{H}_p + \mathcal{H}_V$ in the vicinity of the soluble point.

B. Cubic Model

Largely to simplify the geometry of the presentation, we introduce an alternate model that we find has many of the same properties as its pyrochlore analog. The model is the QDM on the cubic lattice, with *three* dimers touching every site. We consider only the most local dynamics, which rotates the configuration on square plaquettes with two dimers on opposite sides, and the corresponding Rokhsar-Kivelson potential that counts flippable squares. Reversing the mapping above, we can also think of this as a spin model with $S = 1/2$ on the links of a cubic lattice, or, equivalently, on the sites of a lattice of corner-sharing octahedra with their centers at the cubic sites (Fig. 5). The octahedra play the role of the pyrochlore tetrahedra, with the total spin on each $S_{oct}^z = 0$. Denoting cubic sites by boldface letters like \mathbf{r} and identifying the links by pairs like $(\mathbf{r}, \mathbf{x}) \sim (\mathbf{r}, \mathbf{r} + \mathbf{x})$, we can express the dimer kinetic term as a 4-site XY ring exchange for the spins:

$$\mathcal{H}_c = -J_{ring} \sum_{\mathbf{r}} \left(S_{\mathbf{r}x}^+ S_{\mathbf{r}+\mathbf{x},y}^- S_{\mathbf{r}+\mathbf{y},x}^+ S_{\mathbf{r}y}^- + h.c. + \dots \right), \quad (12)$$

where only one orientation of plaquette is shown explicitly. As before, we will be interested in the vicinity of the soluble point of $\mathcal{H}_c + \mathcal{H}_V$.

It is also interesting to note that, as for \mathcal{H}_p , the pure ring exchange model \mathcal{H}_c can be derived as the easy-axis

limit of a Heisenberg antiferromagnet. In this case one begins with spins on the network of corner-sharing octahedra with nearest-neighbor exchange, and an additional exchange of the same sign and magnitude between spins at opposite points of the same octahedron. The Hamiltonian can be written as a sum over octahedra and the analysis proceeds exactly as before.

C. Frustrated $U(1)$ Gauge Theory

Both the cubic and pyrochlore models have an exact $U(1)$ gauge invariance, as is generally the case in dimer models. In the pyrochlore model, this arises because of the local integer conserved quantity S_t^z . The local symmetry is generated by rotations about the z -axis in spin space on all the sites in a given tetrahedron: $G_t(\alpha) = \exp(i\alpha S_t^z)$. These generators commute with one another and the Hamiltonian. It is important to emphasize that this gauge symmetry is generated by *physical* transformations and has nothing to do with any redundancy in our description. These statements also hold for the cubic model, with octahedra substituted for tetrahedra. For now, we shall focus on the cubic model for ease of presentation. All of the statements in this and the following section can be generalized simply to the pyrochlore case; this is summarized in Section II E below.

The gauge structure suggests we may gain insight by thinking about the model as a $U(1)$ lattice gauge theory, an approach that proved helpful in understanding the square lattice QDM²⁵. In fact, it is possible to formally rewrite \mathcal{H}_c as a pure gauge theory on the cubic lattice. To see this, we find it convenient to soften the hardcore constraint on the bosons by explicitly introducing an on-site repulsion term in the Hamiltonian. We also go to quantum rotor variables $n_{\mathbf{r}\mathbf{r}'} \in \mathbb{Z}$ and $\phi_{\mathbf{r}\mathbf{r}'} \in [-\pi, \pi]$, with commutation relations $[\phi_{\mathbf{r}i}, n_{\mathbf{r}'j}] = i\delta_{ij}\delta_{\mathbf{r}\mathbf{r}'}$. Using the relations $S^z = n - 1/2$ and $S^\pm = \exp(\pm i\phi)$, we have

$$\begin{aligned} \mathcal{H}_c = & \frac{U}{2} \sum_{\langle \mathbf{r}\mathbf{r}' \rangle} (n_{\mathbf{r}\mathbf{r}'} - 1/2)^2 \\ & - K \sum_{\square} \cos(\phi_1 - \phi_2 + \phi_3 - \phi_4), \end{aligned} \quad (13)$$

where the numbering inside the cosine proceeds around the perimeter of the given square. This is a faithful representation of the spin model Eq. (12) in the limit $U/K \rightarrow \infty$, which just imposes the hardcore constraint $n_{\mathbf{r}\mathbf{r}'} = 0, 1$.

We now define an orientation on the cubic links, which we take to point out of the A sublattice and into the B sublattice. This allows us to define oriented link variables by:

$$e_{\mathbf{r}\mathbf{r}'} = \pm(n_{\mathbf{r}\mathbf{r}'} - 1/2) \quad (14)$$

$$a_{\mathbf{r}\mathbf{r}'} = \pm\phi_{\mathbf{r}\mathbf{r}'}. \quad (15)$$

Here we take the plus/minus sign when \mathbf{r} lies in the A/B sublattice. Since $e_{\mathbf{r}\mathbf{r}'} = -e_{\mathbf{r}'\mathbf{r}}$, these variables can be

thought of as components of vector fields taken along the links of the lattice. Putting these definitions into the Hamiltonian, we have

$$\mathcal{H}_c = \frac{U}{2} \sum_{\langle \mathbf{r} \mathbf{r}' \rangle} e_{\mathbf{r} \mathbf{r}'}^2 - K \sum_{\square} \cos \left(\sum_{\mathbf{r} \mathbf{r}' \in \square} a_{\mathbf{r} \mathbf{r}'} \right). \quad (16)$$

The sum inside the cosine is taken in an oriented fashion around the links of the given square plaquette, and is thus a discrete line integral of $a_{\mathbf{r} \mathbf{r}'}$ along a smallest possible closed path. This is a lattice version of the curl, so we define:

$$(\text{curl } a)_{\square} = \sum_{\mathbf{r} \mathbf{r}' \in \square} a_{\mathbf{r} \mathbf{r}'}. \quad (17)$$

Eq. (16) is invariant under gauge transformations written in the usual form $a_{\mathbf{r} \mathbf{r}'} \rightarrow a_{\mathbf{r} \mathbf{r}'} + \chi_{\mathbf{r}'} - \chi_{\mathbf{r}}$. Therefore $a_{\mathbf{r} \mathbf{r}'}$ behaves like a vector potential, and since $[a_{\mathbf{r} \mathbf{r}'}, e_{\mathbf{r} \mathbf{r}'}] = i$, $e_{\mathbf{r} \mathbf{r}'}$ plays the role of an electric field. Since the vector potential is a 2π -periodic phase this is evidently a *compact* gauge theory. The “electric” charge is given by the lattice divergence of $e_{\mathbf{r} \mathbf{r}'}$:

$$(\text{div } e)_{\mathbf{r}} = \sum_{\mathbf{r}' \leftarrow \mathbf{r}} e_{\mathbf{r} \mathbf{r}'} = \pm S_{\text{oct}}^z, \quad (18)$$

where the sum is over the sites adjacent to \mathbf{r} . In the ground state there is no gauge charge since $S_{\text{oct}}^z = 0$, and single gauge charges have a large gap of order J_z .

Suppose \mathbf{r} is a site in the A sublattice. Acting with $S_{\mathbf{r}, \mathbf{x}}^+$ creates two octahedra with $S_{\text{oct}}^z = 1$, at \mathbf{r} and $\mathbf{r} + \mathbf{x}$. In the gauge theory language, there is a positive electric charge at \mathbf{r} and a negative one at $\mathbf{r} + \mathbf{x}$, where the sign of the charge comes from the orientation convention Eq. (14). We can now act with the infinite string operator:

$$\mathcal{O}_{\text{string}} = \prod_{n=0}^{\infty} S_{[\mathbf{r} + (n+2)\mathbf{x} + n\mathbf{y}], y}^+ S_{[\mathbf{r} + (n+1)\mathbf{x} + n\mathbf{y}], x}^-. \quad (19)$$

This hops the gauge charge originally at $\mathbf{r} + \mathbf{x}$ off to infinity, leaving an isolated $S^z = 1$ octahedron at \mathbf{r} . The two $S^z = 1$ octahedra together carry $S_{\text{total}}^z = 1$, so the single remaining octahedron is evidently a $S^z = 1/2$ spinon. The spinons are single electric gauge charges and can propagate freely in a deconfining phase of the gauge theory; such a state is therefore fractionalized. We note that, because spinons cannot hop from one sublattice to the other, there are in fact two spinon flavors.

Because the theory is compact, magnetic charge is also allowed. Define dual lattice sites by serif characters $\mathbf{r} = \mathbf{r} + (\mathbf{x} + \mathbf{y} + \mathbf{z})/2$; these are located at the centers of the cubic “boxes” of the direct lattice. The links of the dual lattice are naturally associated with the square plaquettes of the direct lattice. Using this correspondence we define a magnetic field on the dual links by $\pi b_{\mathbf{r} \mathbf{r}'} = (\text{curl } a)_{\square}$. The sense of the lattice curl is given by the right hand rule and the vector $\mathbf{r}' - \mathbf{r}$. The lattice divergence $(\text{div } b)_{\mathbf{r}}$ gives the magnetic charge inside

the box at \mathbf{r} . Naively this divergence vanishes since each term $a_{\mathbf{r} \mathbf{r}'}$ occurs twice, with opposite signs, but this is not the case because b is a periodic variable invariant under $b \rightarrow b + 2$. In fact we have $(\text{div } b)_{\mathbf{r}} = 2n_{\mathbf{r}}$ for integer $n_{\mathbf{r}}$; the magnetic charge is automatically quantized. It is convenient to take $b_{\mathbf{r} \mathbf{r}'} \in [-1, 1]$, so that $n_{\mathbf{r}} = 0, \pm 1, \pm 2$ on each box. It is also possible to have $n_{\mathbf{r}} = -3$ in our convention, but this measure zero point in the configuration space of magnetic fields should be ignored. While electric charges are locally conserved in the low-energy manifold, there is no such conservation law for magnetic charge and we expect $n_{\mathbf{r}} \neq 0$ even in the ground state. While this means the ground state always has some local fluctuations of magnetic charge, it does *not* necessarily contain monopoles, which are smoothly-varying defect configurations unaffected by a small amount of coarse-graining.

The model Eq. (16) looks identical to the standard Hamiltonian formulation of compact $U(1)$ lattice gauge theory, but there is one difference of critical importance in the limit of interest $U/K \rightarrow \infty$. Here, the electric field takes on half-integer rather than integer values. In the case of integer electric fields, the vacuum in the large- U limit is trivial: $e = 0$ everywhere with small fluctuations. In our model this limit enforces the nontrivial constraint $e = \pm 1/2$. This is another expression of the inherent frustration, so we refer to the model as a “frustrated gauge theory.” This situation is essentially the same as that arising in the large- N limit of bipartite $SU(N)$ antiferromagnets^{26,27}, and in the gauge theory description of the square lattice QDM²⁵. There, one considers an integer-valued electric field in a background of static charge; of course, our model can also be viewed this way by making a shift of the electric field.

To gain insight into the possible phases of \mathcal{H}_c , we briefly review the properties of the standard unfrustrated gauge theory, which has the same Hamiltonian as our model but an integer electric field²⁸. There are two phases, separated by a transition at $(U/K)_c \approx 1$. For $U/K > (U/K)_c$, the “strong coupling” side of the transition, the model enters a confining phase smoothly connected to the trivial $U = \infty$ vacuum $e_{\mathbf{r} \mathbf{r}'} = 0$. In this phase all excitations are gapped, and static sources of the electric field are confined by a linear potential. For $U/K < (U/K)_c$ one enters the deconfining Coulomb phase, so named because static gauge charges interact via a $1/r$ Coulomb potential and are thus free to propagate. At low energies, the effective description of the Coulomb phase is simply Gaussian QED, so there is a gapless, linearly dispersing photon with two transverse polarizations.

In the Coulomb phase, magnetic monopoles are gapped and interact via a $1/r$ magnetic Coulomb potential. The monopoles incorporate the compact nature of the magnetic field, which is not important at low energies in the deconfined phase. In the confined phase, however, the magnetic field fluctuates wildly, its periodicity is important, and the monopoles have proliferated and condensed.

This distinguishes the two phases: in the Coulomb phase the monopole propagator decays exponentially, while in the confined phase it goes to a constant. This distinction is more robust than the Wilson loop, which fails to differentiate between the phases in the presence of matter fields.

Returning to the frustrated gauge theory, we can infer that it also has a Coulomb phase at small U/K . This should be so because in the deconfined phase the discrete nature of the electric field is unimportant, so the half-integer nature of $e_{\mathbf{r}\mathbf{r}'}$ will not play a role. We will be interested in whether the Coulomb phase survives in the opposite limit of strong coupling, perhaps stabilized by additional terms in the Hamiltonian.

D. Electric-Magnetic Duality

In recent work on other models with XY ring exchange, it has been useful to make a novel “plaquette duality” transformation^{23,24}. In the case of the frustrated gauge theory, plaquette duality is in fact identical to the more familiar electric-magnetic duality for $U(1)$ gauge theories. We shall make use of the dual cubic lattice defined in the preceding section. We define oriented variables on the dual links $\alpha_{\mathbf{r}\mathbf{r}' \in \pi\mathbb{Z}}$ and $b_{\mathbf{r}\mathbf{r}' \in [-1, 1]}$, which we take to be canonically conjugate: $[b, \alpha] = i$ on the same dual link, zero otherwise. As discussed above, $b_{\mathbf{r}\mathbf{r}'}$ is the magnetic field, defined by:

$$\pi b_{\mathbf{r}\mathbf{r}'} = (\text{curl } a)_{\square}, \quad (20)$$

where the sense of the curl is given by the right hand rule. The conjugate variable will play the role of a “dual vector potential,” and is related to the electric field by:

$$\pi(e_{\mathbf{r}\mathbf{r}'} - e_{\mathbf{r}\mathbf{r}'}^0) = (\text{curl } \alpha)_{\square*}, \quad (21)$$

where the curl is taken around the *dual* square plaquette encircling the direct link joining \mathbf{r} to \mathbf{r}' , and again the orientation is given by the right hand rule. Here $e_{\mathbf{r}\mathbf{r}'}^0 = \pm 1/2$ is a static, divergenceless background field; this is necessary for consistency with $e_{\mathbf{r}\mathbf{r}'} \in \mathbb{Z} + 1/2$. With these definitions, the dual commutation relations are consistent with the original ones.

In dual variables the Hamiltonian is

$$\mathcal{H}_{cd} = \frac{U}{2\pi^2} \sum_{\square*} ((\text{curl } \alpha)_{\square*} + \pi e_{\mathbf{r}\mathbf{r}'}^0)^2 - K \sum_{\langle \mathbf{r}\mathbf{r}' \rangle} \cos(\pi b_{\mathbf{r}\mathbf{r}'}), \quad (22)$$

where the first sum is over dual plaquettes. The constraint of zero electric charge is now automatically satisfied, since $\text{div } e = \text{div}(e^0 + \text{curl } \alpha/\pi) = 0$. However, magnetic charge can take on continuous values in the dual variables, and one should impose the constraint $\text{div } b \in 2\mathbb{Z}$. This constraint commutes with \mathcal{H}_{cd} since it is invariant under the dual gauge transformations $\alpha_{\mathbf{r}\mathbf{r}'} \rightarrow \alpha_{\mathbf{r}\mathbf{r}'} + \lambda_{\mathbf{r}} - \lambda_{\mathbf{r}'}$, where $\lambda_{\mathbf{r}} \in \pi\mathbb{Z}$. Note that because

magnetic charge is not locally conserved, we are not allowed to demand $\text{div } b = 0$.

It is useful, and enlightening, to write down the Euclidean action obtained by a Trotter expansion in eigenstates of the dual vector potential. As usual, one begins with the partition function

$$Z_{cd} = \text{Tr} \left(\exp(-\beta \mathcal{H}_{cd}) \mathcal{P} \right). \quad (23)$$

Here $\mathcal{P} = \prod_r \mathcal{P}_r$ is a projection operator imposing the quantization of magnetic charge:

$$\begin{aligned} \mathcal{P}_r &= \sum_{\alpha_{\mathbf{r}\mathbf{r}'} \in \pi\mathbb{Z}} \delta((\text{div } b)_r - 2\alpha_{\mathbf{r}\mathbf{r}}/\pi) \\ &= \frac{1}{2} \sum_{\alpha_{\mathbf{r}\mathbf{r}'} \in \pi\mathbb{Z}} \exp(i\alpha_{\mathbf{r}\mathbf{r}}(\text{div } b)_r). \end{aligned} \quad (24)$$

Breaking the exponential in Eq. (23) into $N_\tau = \beta/\epsilon$ timeslices, and inserting \mathcal{P} once in every timeslice, one has:

$$Z_{cd} = \text{Tr} \left(\exp(-\epsilon \mathcal{H}_{cd}) \mathcal{P} \right)^{N_\tau} \quad (25)$$

$$= \sum_{\{\alpha_{r\mu}(\tau)\}} \exp(-\mathcal{S}_{cd}), \quad (26)$$

where the index $\mu = \tau, x, y, z$. The imaginary time component of α_μ comes from the Poisson-resummed form of the projector Eq. (24). The spatial components enter as the eigenvalues of the states $|\{\alpha_{ri}(\tau)\}\rangle$ used to form the resolution of the identity at each timeslice. Following very similar manipulations to those in Appendix A of Ref. (23), one obtains the dual action:

$$\begin{aligned} \mathcal{S}_{cd} &= \frac{1}{\pi^2} \ln \left(\frac{2}{\epsilon K} \right) \sum_{\tau, \langle \mathbf{r}\mathbf{r}' \rangle} \left(\Delta_\tau \alpha_{\mathbf{r}\mathbf{r}'} + \alpha_{\mathbf{r}\mathbf{r}} - \alpha_{\mathbf{r}'\mathbf{r}'} \right)^2 \\ &+ \frac{\epsilon U}{2\pi^2} \sum_{\tau, \square*} \left((\text{curl } \alpha)_{\square*} + \pi e_{\mathbf{r}\mathbf{r}'}^0 \right)^2, \end{aligned} \quad (27)$$

where $\Delta_\tau f \equiv f(\tau + \epsilon) - f(\tau)$.

The action Eq. (27) is essentially a higher-dimensional generalization of the height model partition function arrived at by similar manipulations in the context of the square lattice QDM²⁵. Significantly, it differs in having a local rather than a global invariance, under spacetime-dependent dual gauge transformations of the form $\alpha_\mu \rightarrow \alpha_\mu + \Delta_\mu \lambda$. In fact, except for the (important) discrete nature of the fields, \mathcal{S}_{cd} has the same structure as non-compact lattice QED. In Sec. III below, it will be useful to imagine softening the constraint of discreteness on the fields to interpolate between the dual partition function and an effective description of the Coulomb phase.

E. Pyrochlore Gauge Theory and Duality

We now return to the pyrochlore ring model \mathcal{H}_p . In this case the diamond lattice with sites at the centers of

the tetrahedra (discussed in Sec. II A) plays the role the cubic lattice did for the cubic model. Denoting *diamond* sites by boldface characters, we soften the hardcore constraint on the bosons and go to quantum rotor variables living on the diamond links:

$$\begin{aligned} \mathcal{H}_p = & \frac{U}{2} \sum_{\langle \mathbf{r} \mathbf{r}' \rangle} (n_{\mathbf{r} \mathbf{r}'} - 1/2)^2 \\ & - K \sum_{\bigcirc} \cos(\phi_1 - \phi_2 + \phi_3 - \phi_4 + \phi_5 - \phi_6). \end{aligned} \quad (28)$$

Here the second sum is over the hexagonal loops of the diamond lattice (Fig. 4), and the numbering inside the cosine proceeds around the perimeter of the given hexagon. The diamond lattice is bipartite, so we define an orientation by declaring that links naturally point out of the “up-pointing” sites and into the “down-pointing” ones (corresponding to up- and down-pointing tetrahedra, respectively). We define an oriented electric field and vector potential exactly as in Eqs. (14,15). The Hamiltonian then takes the form of the diamond lattice frustrated gauge theory:

$$\mathcal{H}_p = \frac{U}{2} \sum_{\langle \mathbf{r} \mathbf{r}' \rangle} e_{\mathbf{r} \mathbf{r}'}^2 - K \sum_{\bigcirc} \cos \left(\sum_{\mathbf{r} \mathbf{r}' \in \bigcirc} a_{\mathbf{r} \mathbf{r}'} \right). \quad (29)$$

It is evident that the lattice curl now naturally lives on the hexagons of the diamond lattice.

Again the electric charge has a simple interpretation in the spin language:

$$(\text{div } e)_{\mathbf{r}} = \pm S_{\mathbf{r}}^z. \quad (30)$$

Tetrahedra with $S_{\mathbf{r}}^z = \pm 1$ are now the $S^z = 1/2$ spinons carrying unit gauge charge. Single spinons can be created by a string operator similar to Eq. (19). For small U/K the model should again enter a deconfining phase where the spinons are free to propagate.

We define a dual lattice of plaquette variables by putting a site at the center of every pyrochlore hexagon. This is also a pyrochlore lattice, and it will be useful to think of its sites as the links of a dual diamond lattice with sites labelled by serif characters \mathbf{r} . Each hexagon of the dual lattice encircles a link of the direct lattice, and vice versa. As before, magnetic charge lives on the dual lattice sites. The dual variables, again with the commutator $[b, a] = i$ on the same link, are defined on the dual links by:

$$\pi(e_{\mathbf{r} \mathbf{r}'} - e_{\mathbf{r} \mathbf{r}'}^0) = (\text{curl } \alpha)_{\bigcirc^*} \quad (31)$$

$$\pi b_{\mathbf{r} \mathbf{r}'} = (\text{curl } a)_{\bigcirc}, \quad (32)$$

with the sense of the lattice curls determined by the right hand rule as usual. Here $(\text{div } b)_{\mathbf{r}} = 2n_{\mathbf{r}}$, with $n_{\mathbf{r}} = 0, \pm 1$. The Hamiltonian takes the form

$$\mathcal{H}_{pd} = \frac{U}{2\pi^2} \sum_{\bigcirc^*} ((\text{curl } \alpha)_{\bigcirc^*} + \pi e_{\mathbf{r} \mathbf{r}'}^0)^2 - K \sum_{\langle \mathbf{r} \mathbf{r}' \rangle} \cos(\pi b_{\mathbf{r} \mathbf{r}'}) \quad (33)$$

One can derive an action in eigenstates of the dual vector potential as in the previous section, with the result:

$$Z_{pd} = \sum_{\{\alpha_{\mathbf{r} \mathbf{r}'}(\tau)\}} \sum_{\{\alpha_{\mathbf{r} \tau}(\tau)\}} \exp(-\mathcal{S}_{pd}), \quad (34)$$

and

$$\begin{aligned} \mathcal{S}_{pd} = & \frac{1}{\pi^2} \ln \left(\frac{2}{\epsilon K} \right) \sum_{\tau, \langle \mathbf{r} \mathbf{r}' \rangle} \left(\Delta_{\tau} \alpha_{\mathbf{r} \mathbf{r}'} + \alpha_{\mathbf{r} \tau} - \alpha_{\mathbf{r}' \tau} \right)^2 \\ & + \frac{\epsilon U}{2\pi^2} \sum_{\tau, \bigcirc^*} \left((\text{curl } \alpha)_{\bigcirc^*} + \pi e_{\mathbf{r} \mathbf{r}'}^0 \right)^2. \end{aligned} \quad (35)$$

The constraint of magnetic charge quantization $(\text{div } b)_{\mathbf{r}} \in 2\mathbb{Z}$ enters as before, giving rise to the temporal dual vector potential fields in Z_{pd} .

III. EFFECTIVE THEORY

A. Coulomb Phase Effective Action

It is well-known that the low-energy description of the Coulomb phase of compact $U(1)$ gauge theory is non-compact QED with no matter fields. In our case it will be convenient to work in dual variables to formulate the effective theory, which more naturally allows the inclusion of magnetic charge fluctuations. Depending on the purpose at hand, different formulations of the effective action will be useful. To fix notation, we show them all here. In each case the partition function is of the form:

$$\mathcal{Z}^0 = \prod_{\tau} \prod_{\mathbf{r}, \mu} \int [d\tilde{\alpha}_{\mathbf{r}, \mu}(\tau)] \exp(-\mathcal{S}^0), \quad (36)$$

where $\tilde{\alpha}$ is a real-valued field. It will often be convenient to keep the full spatial lattice structure, in which case we can define $\tilde{\alpha}$ in terms of the microscopic variables by the *temporal* coarse-graining:

$$\tilde{\alpha}_{\mathbf{r} \mu} = [\alpha_{\mathbf{r} \mu}]_f - \frac{\alpha_{\mathbf{r} \mu}^0}{2}. \quad (37)$$

The brackets $[\cdot]_f$ denote an average over high-frequency modes in imaginary time, and we have subtracted the time-independent, non-fluctuating background $\alpha_{\mathbf{r} \mu}^0 \in \pi\mathbb{Z}$ defined by:

$$\frac{1}{\pi} (\text{curl } \alpha^0)_{\bigcirc^*} = -2e_{\mathbf{r} \mathbf{r}'}^0, \quad (38)$$

with $\tilde{\alpha}_{\mathbf{r} \tau}^0 = 0$. If (as we always do in practice) we restrict attention to spatially periodic $e_{\mathbf{r} \mathbf{r}'}^0$ with zero average electric flux in every direction, α^0 can also be taken periodic. This subtraction simplifies the relation between the electric field and dual vector potential, since

$$\pi e_{\mathbf{r} \mathbf{r}'} = (\text{curl } (\alpha - \alpha^0/2))_{\bigcirc^*}. \quad (39)$$

On a spacetime lattice, the action looks almost identical to \mathcal{S}_{cd} in Eq. (27):

$$\begin{aligned}\mathcal{S}_{lat}^0 &= \frac{g_\tau}{2} \sum_\tau \sum_{\langle rr' \rangle} (\Delta_\tau \tilde{\alpha}_{rr'} + \tilde{\alpha}_{rr} - \tilde{\alpha}_{r'r})^2 \quad (40) \\ &+ \frac{g_s}{2} \sum_\tau \sum_{\square^*} (\text{curl } \tilde{\alpha})^2.\end{aligned}$$

The only difference from the microscopic model is that the fields are now continuous. We will also have occasion to retain the spatial lattice structure but take the time-continuum limit, in which case we write

$$\begin{aligned}\mathcal{S}_{tc}^0 &= \frac{1}{2\mathcal{K}} \int_\tau \sum_{\langle rr' \rangle} (\partial_\tau \tilde{\alpha}_{rr'} + \tilde{\alpha}_{rr} - \tilde{\alpha}_{r'r})^2 \quad (41) \\ &+ \frac{\mathcal{U}}{2} \int_\tau \sum_{\square^*} (\text{curl } \tilde{\alpha})^2.\end{aligned}$$

The parameters here are related to those in Eq. (40) by $\mathcal{K} = (\epsilon g_\tau)^{-1}$ and $\mathcal{U} = g_s/\epsilon$, and $\tilde{\alpha}_{rr}$ now has units of inverse time. This action corresponds to the effective dual Hamiltonian (in the sector with no magnetic charge):

$$\mathcal{H}^0 = \frac{\mathcal{K}}{2} \sum_{\langle rr' \rangle} \tilde{b}_{rr'}^2 + \frac{\mathcal{U}}{2} \sum_{\square^*} (\text{curl } \tilde{\alpha})^2, \quad (42)$$

which can be obtained simply by expanding the cosine in Eq. (22). The lattice effective actions for the pyrochlore model look identical to Eqs. (40, 41), where the only change necessary is the replacement of the sums over dual square plaquettes with sums over dual hexagons.

Finally, in order to take the spatial continuum limit, we introduce a continuum 4-vector field $\Upsilon_\mu(\mathbf{r}, \tau)$, formally defined by the replacements

$$\begin{aligned}\tilde{\alpha}_{ri} &\rightarrow a(\mathbf{e}_i \cdot \boldsymbol{\Upsilon}) \quad (43) \\ \tilde{\alpha}_{rr} &\rightarrow \Upsilon_\tau.\end{aligned}$$

Here \mathbf{e}_i are the vectors connecting the site \mathbf{r} to its nearest neighbors, in either the cubic or diamond lattice. Naively it seems we have thrown away too much information in the pyrochlore case, since there are four sites per unit cell, but only three spatial components of the continuum vector field. However, there are also *two* gauge degrees of freedom per unit cell of the diamond lattice, corresponding to changing $(\text{div } \alpha)_r$ on the two different sublattices. This leaves us with two transverse degrees of freedom, the same number as in the cubic model and the continuum theory. The full spacetime continuum theory is

$$\begin{aligned}\mathcal{S}_{stc}^0 &= \frac{1}{2\mathcal{K}_c} \sum_i \int_{\tau, \mathbf{r}} (\partial_\tau \Upsilon_i - \partial_i \Upsilon_\tau)^2 \quad (44) \\ &+ \frac{\mathcal{U}_c}{2} \sum_{i < j} \int_{\tau, \mathbf{r}} (\partial_i \Upsilon_j - \partial_j \Upsilon_i)^2,\end{aligned}$$

where $\mathcal{K}_c = \mathcal{K}a$ and $\mathcal{U}_c = \mathcal{U}a$ (a is a microscopic length). The spatial/temporal components of Υ_μ have units of inverse length/time. The form is identical to the familiar

(dual) Maxwell action for electromagnetism with photon velocity $v_p = \sqrt{\mathcal{U}_c \mathcal{K}_c}$. This action can be used to obtain long-wavelength properties of the Coulomb phase of either microscopic model, but at the end of any calculation the allowed spatial components of all vector fields are determined by the lattice structure.

To calculate using any of these effective actions, it is convenient to implement a gauge-fixing procedure. The well-known manipulations of Faddeev and Popov²⁹ tell us that we may add any function of the vector potential 4-divergence to the action. The standard choice, in our nonstandard notation, is:

$$\mathcal{S}_{FP} = \frac{1}{2\mathcal{E}\mathcal{U}_c \mathcal{K}_c^2} \int_{\tau, \mathbf{r}} (\partial_\tau \Upsilon_\tau + v_p^2 \nabla \cdot \boldsymbol{\Upsilon})^2. \quad (45)$$

If we choose $\xi = 1$, as usual the off-diagonal terms in the action are cancelled and we obtain the simple photon propagator:

$$\langle \Upsilon_\mu(\mathbf{k}, \omega_n) \Upsilon_\nu(\mathbf{k}', \omega'_n) \rangle = \frac{(2\pi)^4 \delta(\omega_n + \omega'_n) \delta(\mathbf{k} + \mathbf{k}') \mathcal{K}_c g_{\mu\nu}}{\omega_n^2 + v_p^2 k^2}, \quad (46)$$

where the Euclidean metric is defined by $g_{\tau\tau} = v_p^2$, $g_{\tau i} = g_{i\tau} = 0$ and $g_{ij} = \delta_{ij}$. While these expressions hold in the continuum, it is amusing to note that the obvious lattice regularization of Eq. (45) also cancels all off-diagonal terms on the cubic lattice. Working in the time-continuum action, we find the lattice propagator:

$$\langle \tilde{\alpha}_\mu(\mathbf{k}, \omega_n) \tilde{\alpha}_\nu(\mathbf{k}', \omega'_n) \rangle = \frac{(2\pi)^4 \delta(\omega_n + \omega'_n) \delta(\mathbf{k} + \mathbf{k}') \mathcal{K} g_{\mu\nu}}{\omega_n^2 + \mathcal{U} \mathcal{K} g(\mathbf{k})}, \quad (47)$$

where $g(\mathbf{k}) = 2 \sum_i (1 - \cos k_i)$. On the diamond lattice, even more complicated Faddeev-Popov terms seem only to cancel some of the off-diagonal terms.

Finally, it is important to note that this procedure is only legitimate for calculating expectation values of operators invariant under *continuous* dual gauge transformations. Terms with only discrete dual gauge invariance (see Sec. III C) must be handled more carefully; this issue arises in calculating the monopole propagator in Section IV D.

B. RK Point Effective Action

At the Rokhsar-Kivelson point, we find that both models are described by the effective action

$$\begin{aligned}\mathcal{S}_{RK}^0 &= \frac{1}{2\mathcal{K}_c} \sum_i \int_{\tau, \mathbf{r}} (\partial_\tau \Upsilon_i - \partial_i \Upsilon_\tau)^2 \quad (48) \\ &+ \frac{\mathcal{W}_c}{2} \int_{\tau, \mathbf{r}} (\nabla \times (\nabla \times \boldsymbol{\Upsilon}))^2.\end{aligned}$$

The “stiffness” term for the electric field has vanished, and while the theory remains gauge invariant, the photon dispersion now vanishes *quadratically*: $\omega \sim \mathbf{k}^2$. The

\mathcal{U}_c term is relevant, as can be seen by the usual power-counting procedure, so this action cannot describe a stable phase. A small positive \mathcal{U}_c will drive the system into the Coulomb phase, while a small negative \mathcal{U}_c will result in an electric field “crystal;” in the dimer language this is a state with long-range dimer order and no flippable plaquettes. As we argue in Section V, precisely this picture describes the physics of the microscopic models near the RK point, with the relation $\mathcal{U}_c \propto (1 - V/J_{ring})$.

A very similar story is known to apply to the $d = 2$ square lattice QDM²⁰. In that case, electric-magnetic duality leads to a height model partition function, which describes the fluctuations of a discrete field living on the square lattice plaquettes in 2+1 dimensions. Just as above, softening the constraint of discreteness naturally leads to the Gaussian effective action:

$$\mathcal{S}_{height} = \int d\tau d^2\mathbf{r} \left((\partial_\tau h)^2 + \kappa_1 (\nabla h)^2 + \kappa_2 (\nabla^2 h)^2 \right). \quad (49)$$

When $\kappa_1 = 0$ we have a description of the RK point, which has power-law dimer-dimer correlations. For small negative κ_1 the system goes into the staggered valence bond crystal state. These have natural analogs in the three-dimensional case. However, a small positive κ_1 leads to the columnar state (via an instability of the Gaussian theory), with long range dimer-dimer correlations and a maximal number of flippable plaquettes. This occurs because Eq. (49) with $\kappa_1 > 0$ would describe the unstable Coulomb phase of 2+1-dimensional $U(1)$ gauge theory. In three dimensions, however, the analogous phase is stable and should exist adjacent to the RK point.

To calculate with Eq. (48) we again carry out a gauge-fixing procedure. We add the Faddeev-Popov term:

$$\mathcal{S}_{FPP} = \frac{1}{2\xi\mathcal{K}_c^3} \int_{\tau, \mathbf{r}} (\partial_\tau \Upsilon_\tau + \mathcal{K}_c^2 \nabla \cdot \Upsilon)^2. \quad (50)$$

Although this does not cancel all off-diagonal terms, it leads to the relatively simple photon propagator:

$$\begin{aligned} & \langle \Upsilon_\mu(\mathbf{k}, \omega_n) \Upsilon_\nu(\mathbf{k}', \omega'_n) \rangle \\ &= (2\pi)^4 \delta(\omega_n + \omega'_n) \delta(\mathbf{k} + \mathbf{k}') \mathcal{K}_c \mathcal{M}_{\mu\nu}(\mathbf{k}, \omega_n), \end{aligned} \quad (51)$$

where

$$\begin{aligned} \mathcal{M}_{\tau\tau} &= \mathcal{K}_c^2 / (\omega_n^2 + \mathcal{K}_c^2 k^2) \\ \mathcal{M}_{\tau i} &= \mathcal{M}_{i\tau} = 0 \\ \mathcal{M}_{ii} &= \frac{1}{f(\omega_n, \mathbf{k})} [m^2 \omega_n^2 + k_i^2 k^2 + m^2 \mathcal{K}_c^2 (k^2 - k_i^2)] \\ \mathcal{M}_{ij} &= \frac{1}{f(\omega_n, \mathbf{k})} [k_i k_j (k^2 - \mathcal{K}_c^2 m^2)] \quad (i \neq j), \end{aligned} \quad (52)$$

and

$$f(\omega_n, \mathbf{k}) = (\omega_n^2 + \mathcal{K}_c^2 k^2)(m^2 \omega_n^2 + k^4), \quad (53)$$

with $m = (\mathcal{K}_c \mathcal{W}_c)^{-1/2}$.

C. Corrections

While all gauge-invariant corrections to \mathcal{S}_{stc}^0 are irrelevant in the renormalization group sense, in order to understand the detailed realization of the $U(1)$ spin liquid (and the nearby RK point) in any microscopic model it will generally be important to consider corrections to the effective action. Furthermore, we need to specify relations between the microscopic and effective degrees of freedom. Naïvely we could write $\alpha_\mu \sim \tilde{\alpha}_\mu + \alpha_\mu^0/2$, but any corrections allowed by symmetry will generically be present.

For ease of presentation, we focus on the cubic model; the lattice structure is unimportant for these results. The symmetries of the microscopic model are listed in detail in Appendix A. It is important to note that, because the background α^0 is not invariant under all lattice symmetries, the dual vector potential transforms with additional shifts under these operations. Furthermore, the dual effective degrees of freedom $\tilde{\alpha}$ and \tilde{b} transform exactly as their microscopic counterparts.

Rather than attempt a painstaking enumeration of all allowed corrections to \mathcal{S}^0 , we discuss some representative examples. The corrections naturally fall into two classes; those invariant under *continuous* dual gauge transformations, and those not. In Hamiltonian language on the lattice, some typical terms in the first class are:

$$\begin{aligned} \mathcal{H}^1 &= \frac{\mathcal{W}}{2} \sum_{\square} (\text{curl } \tilde{e})^2 + \mathcal{W}' \sum_{\square^*} (\text{curl } \tilde{b})^2 \\ &+ \mathcal{U}' \sum_{\langle \mathbf{r} \mathbf{r}' \rangle} \tilde{e}_{\mathbf{r}'}^4 + \mathcal{K}' \sum_{\langle \mathbf{r} \mathbf{r}' \rangle} \tilde{b}_{\mathbf{r}'}^4 + \dots \end{aligned} \quad (54)$$

Terms involving discrete line integrals of both vector potentials around closed loops larger than single plaquettes are also allowed, as are terms containing the divergence of the fields. While these terms are irrelevant, they can have quantitative effects, presumably accessible in perturbation theory. All such corrections are also irrelevant at the RK point, except the \mathcal{W} term, which contributes to the \mathcal{W}_c term in Eq. (48).

More interesting are those terms lacking continuous dual gauge invariance. Here we only consider the single site terms; in the spacetime lattice action these take the form:

$$\begin{aligned} \mathcal{S}^2 &= - \sum_{\tau, \langle \mathbf{r} \mathbf{r}' \rangle} \sum_{q=1}^{\infty} v_{2q} \cos^q(\alpha_{\mathbf{r}\mathbf{r}'}^0) \cos(2q\tilde{\alpha}_{\mathbf{r}\mathbf{r}'}) \\ &- \sum_{\tau, \mathbf{r}} \sum_{q=1}^{\infty} v_{2q}^\tau \cos(2q\tilde{\alpha}_{\tau\mathbf{r}}). \end{aligned} \quad (55)$$

In the first term the α^0 -dependence is necessary to compensate the shifts in $\tilde{\alpha}$ under lattice symmetries. With appropriate choices of coefficients, when these corrections become large they have the effect of pinning the dual vector potential to take on discrete values. This allows

us to interpolate explicitly between the effective theory \mathcal{S}_{lat}^0 and the microscopic partiton function. Physically, the spatial v_{2q} part of \mathcal{S}^2 is a *magnetic charge hopping* term. Its temporal companion is related to the discreteness of magnetic charge. Therefore, these corrections introduce magnetic charge fluctuations into the effective theory. As should be expected when magnetic monopoles are gapped, when these fluctuations are small there is no associated instability. Formally, this should be the case because the correlation functions of $\cos(2q\tilde{\alpha}_\mu)$ are local in space and time. For example,

$$\left\langle \cos(2\tilde{\alpha}_{rr}(\tau)) \cos(2\tilde{\alpha}_{rr'}(\tau')) \right\rangle_0 \propto \delta_{rr'} \delta_{\tau\tau'}, \quad (56)$$

because continuous dual gauge invariance in \mathcal{S}^0 makes each cosine into an independent random variable.

Finally, we consider corrections to the scaling equalities between microscopic and effective degrees of freedom. Some representative contributions in the case of the dual vector potential are, in operator language:

$$\begin{aligned} \alpha_{rr'} &\sim (\tilde{\alpha}_{rr'} + \alpha_{rr'}^0/2) \\ &+ \sum_{q=1}^{\infty} c_{2q} \cos^q(\alpha_{rr'}^0) \sin(2q\tilde{\alpha}_{rr'}) \\ &+ \sum_{n,m=0}^{\infty} c_{n,m}^1 (\tilde{b}_{rr'})^{2n} (\text{curl } \tilde{e})_{\square}^{2m+1} + \dots \end{aligned} \quad (57)$$

This should really be interpreted as an instruction for what effective theory operators to use in the calculation of gauge invariant expectation values. These corrections are not important, and we will neglect them: the second term clearly only leads to local corrections, while the third term and others like it lead only to subdominant power laws, which will always be present on the lattice. The conclusion is the same for corrections to the magnetic field, but for completeness we show some of the representative terms:

$$\begin{aligned} e^{ib_{rr'}} &\sim \exp \left(i \tilde{b}_{rr'} \right) \\ &+ i \sum_{n,m=0}^{\infty} d_{n,m}^1 (\text{curl } \tilde{e})_{\square}^{2n} (\tilde{b}_{rr'})^{2m+1} + \dots \\ &\cdot \left\{ 1 + \sum_{q=1}^{\infty} d_{2q} \cos^q(\alpha_{rr'}^0) \cos(2q\tilde{\alpha}_{rr'}) + \dots \right\} \end{aligned} \quad (58)$$

IV. PROPERTIES OF THE $U(1)$ SPIN LIQUID

Using the effective theory developed above, we now treat some of the more striking properties of the $U(1)$ spin liquid. We focus on its realization in our microscopic models, in the extreme easy-axis limit; a finite but large J_z would introduce small fluctuations of *electric* gauge charge in the ground state. While this does not affect universal properties, it can matter for the correlation functions of some microscopic operators. This

can be understood formally by a more sophisticated execution of the perturbation theory in J_\perp that accounts for splitting of the low-energy manifold and mixing of higher states on an equal footing³⁰. The main result is that the problem at finite J_z can be mapped, by a unitary transformation, order-by-order in J_\perp onto a transformed Hamiltonian acting only within the low-energy manifold where $S_t^z = 0$. The resulting point of view, which may be of general conceptual significance in understanding phases with emergent gauge structure, is that the low-energy sector of the model is unitarily equivalent to a $U(1)$ gauge theory. This mapping also generates non-trivial perturbative relations between physical and transformed operators; however, we ignore these corrections for simplicity.

A. Excitations and Emergent Long-Range Interactions

As already mentioned, the $U(1)$ spin liquid supports a gapped $S^z = 1/2$ spinon carrying electric gauge charge, a gapped topological point defect that plays the role of a magnetic monopole, and a gapless, linearly dispersing “photon” with velocity v_p . The spinon was discussed in Section II C, and in the microscopic models takes the form of a tetrahedron (or octahedron) carrying nonzero S^z . The gap to the spinons is very large, of order J_z .

The monopole is a classical configuration of the magnetic field emanating from a point with nonzero magnetic charge at \mathbf{r}_0 . For a compact gauge field on, say, the cubic lattice, the classical configuration is given by minimizing

$$E[\mathcal{A}] = - \sum_{\langle rr' \rangle} \cos(\pi \mathcal{B}_{rr'}) \quad (59)$$

in the presence of a specified distribution of magnetic charge, which enters via the constraint $(\text{div } \mathcal{B})_r = 2\delta_{rr_0}$. In these expressions $\pi \mathcal{B}_{rr'} = (\text{curl } \mathcal{A})_{\square}$. Far from the center of the monopole the magnetic field will be small, the energy is approximately a sum over $\mathcal{B}_{rr'}^2$, and the minimum is obtained by solving the (discrete) Laplace equation of classical electrostatics. The compact nature of the theory only modifies the field near the core.

In the effective theory, we can create a monopole with the operator

$$\tilde{m}_{r_0}^\dagger = \exp(i \sum_{\langle rr' \rangle} \mathcal{B}_{rr'} \tilde{\alpha}_{rr'}). \quad (60)$$

Because magnetic charge is created at \mathbf{r}_0 , this operator is *not* invariant under continuous dual gauge transformations. The monopole gap is of order \mathcal{K} , and in the microscopic models is likely to be of order J_{ring} as long as \mathcal{K} does not renormalize too much from its bare value. Therefore the monopoles have a much smaller gap than the spinons.

Using the correspondence between microscopic and effective variables, we can write down a creation operator that should have at least some overlap with the true microscopic monopole eigenstate:

$$m_{\mathbf{r}_0}^\dagger = \exp(i \sum_{\langle \mathbf{r} \mathbf{r}' \rangle} \mathcal{A}_{\mathbf{r} \mathbf{r}'} e_{\mathbf{r} \mathbf{r}'}). \quad (61)$$

This is written in terms of the direct variables to connect with the spin language, where the monopoles are defect configurations in the XY component of the spin. Because of the half-integer electric field, the sign of m^\dagger is changed by a 2π -shift of any one of the $\mathcal{A}_{\mathbf{r} \mathbf{r}'}$. However, this overall sign does not fluctuate since the electric fields change only by integer steps.

Both the monopoles and spinons feel an emergent $1/r$ interaction, even though the microscopic Hamiltonians contain only local operators. Consider the field due to a configuration of a few static electric gauge charges (the same discussion could be repeated for magnetic charge). This is given by solving Poisson's equation $\nabla \cdot \mathbf{E} = \sum_i q_i \delta(\mathbf{r} - \mathbf{r}_i)$ to obtain Coulomb's Law. By gauge invariance the longitudinal part of \mathbf{E} does not fluctuate, so the field is simply given by its classical value plus *transverse* fluctuations. This zero point energy does not contribute to the energy difference between the charged state and the charge-free ground state, and one recovers the familiar $1/r$ Coulomb potential. In the RK point effective theory, this interaction is absent for the spinons, but still present for monopoles, because there is no energy cost for longitudinal electric fields.

A word about the statistics of the charged excitations is in order. Certainly, both monopoles and electric charges as discussed above are bosonic. However, a simple argument shows that a *dyon*, a bound state of electric and magnetic charge, has Fermi statistics³¹. If such bound states exist and have lower energy than pure electric charges, then one could say that there are fermionic spinons. While this is a nonuniversal question with no bearing on the low-energy physics, it can be relevant in understanding the possible transitions out of the $U(1)$ spin liquid. The emergence of Fermi statistics in local bosonic models is also of great conceptual interest³², although in the present case it is not clear what, if any, local microscopic interaction will bind electric and magnetic charge.

Finally we turn to the photon. In terms of the spins, it is a linearly dispersing $S^z = 0$ collective mode oscillating between the Ising and XY parts of the spin vector. As for *phonons*, these gapless excitations make the contribution to the low-temperature specific heat $C_{\text{photon}}(T) \propto (T/v_p)^3$. Since in real materials it should be possible to quantitatively understand the phonon contribution to $C(T)$ by measurement of elastic moduli³³, this signature of the $U(1)$ spin liquid should be easily accessible to experiments. Other potential, though likely more delicate, probes of the photon are low-temperature thermal conductivity and Raman scattering. Finally, the

photon manifests itself in the power-law correlations discussed in Section IV C.

B. $U(1)$ Topological Order

In the theory of Z_2 -fractionalized phases, the notion of topological ground state degeneracy⁵ has been very useful both as a conceptual tool, and as a property that can be directly probed by experiments^{6,13,14,15}. The degeneracy is associated with the topological sectors of a deconfining Z_2 gauge field, so it is natural to ask about the generalization of these ideas to $U(1)$ -fractionalized states.

We will work with the microscopic Hamiltonian of cubic frustrated gauge theory (Eq. 16) on a 3-torus, a cube with L lattice sites on a side and periodic boundary conditions:

$$\begin{aligned} e_{[\mathbf{r} + L\mathbf{e}_i],j} &= e_{\mathbf{r}j} \\ \exp(ia_{[\mathbf{r} + L\mathbf{e}_i],j}) &= \exp(ia_{\mathbf{r}j}). \end{aligned} \quad (62)$$

We define an operator to measure the electric flux through a plane perpendicular to each of the three independent cycles of the torus. For example,

$$\Phi_x^E = \sum_{n_y, n_z=0}^{L-1} e_{[n_y \mathbf{y} + n_z \mathbf{z}], x}, \quad (63)$$

with similar definitions for Φ_y^E and Φ_z^E . These fluxes are constants of the motion, and are in fact conserved by *any* local, gauge invariant dynamics. Furthermore, because there is no electric charge in the ground state, by Gauss' Law we can make arbitrary incremental deformations of the specified plane without changing the flux. These fluxes define the electric topological sectors of the gauge theory³⁴.

Now imagine the model is in the Coulomb phase, where in the ground state $\Phi_i^E = 0$. We imagine threading one quantum Φ_0^E of electric flux through the system in, say, the x -direction. Because the energy is proportional to $\int_{\mathbf{r}} \mathbf{E}^2$, the most favorable situation is for the flux to spread itself uniformly through the system, so that $E_x = \Phi_0^E/L^2$. This electric field is purely longitudinal and does not fluctuate, so there is a total energy cost $\mathcal{E} \sim \mathcal{U}_c(\Phi_0^E)^2/L$. Therefore, in the thermodynamic limit, all states with a finite number of electric flux quanta threading each direction of the 3-torus become degenerate with the ground state. Just as in the case of Z_2 topological order, these states are locally identical to the ground state (local correlation functions will be unaffected), but globally distinct.

What about *magnetic* topological sectors of the gauge field? Because $[b_{\mathbf{r} \mathbf{r}'}, \Phi_i^E] = 0$, these can clearly be specified simultaneously with the electric sectors. We define magnetic fluxes Φ_i^B just as above:

$$\Phi_x^B = \sum_{n_y, n_z=0}^{L-1} b_{[n_y \mathbf{y} + n_z \mathbf{z}], x}, \quad (64)$$

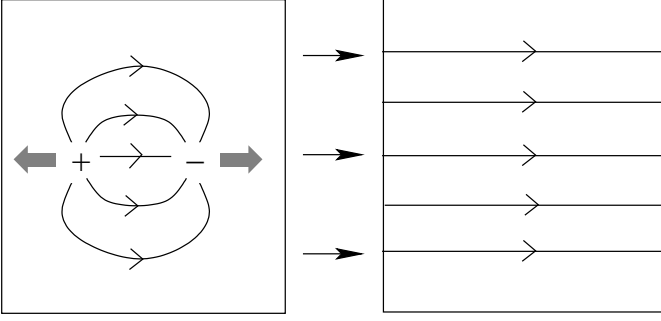


FIG. 6: Illustration of threading a magnetic flux quantum through one direction of a periodic system by creating a monopole-antimonopole pair (left), and moving it apart until the charges return to the same position and annihilate. One is left with no monopoles, and magnetic flux threading the system (right).

and similarly for $\Phi_{y,z}^B$. This expression is a (lattice) surface integral over a plane bisecting the system, which has the topology of a 2-torus due to the periodic boundary conditions. Because this is a closed surface and b is the curl of a compact vector potential, the magnetic flux is quantized: $\Phi_i^B = 2n_i^B$.

However, there is an important difference from the case of electric flux: because magnetic charge fluctuates in the ground state, Φ_i^B is *not* a constant of the motion in the microscopic theory. Within the Coulomb phase, though, the magnetic flux defined in the effective theory does commute with \mathcal{H}^0 , the effective Hamiltonian written in dual variables. Magnetic charge fluctuations can mix states with different values of the flux by creating a monopole-antimonopole pair and separating the particles along one lattice direction, only to have them annihilate when they complete their periodic journey around the system (Fig. 6). Because the monopoles are gapped, the rate for this process is suppressed exponentially in the system size, and it does not occur for a large enough sample. As with the electric sectors, the magnetic flux sectors become degenerate ground states as $L \rightarrow \infty$ with energies scaling to zero as $1/L$. In the microscopic theory, we expect that $\langle \Phi_i^B \rangle$ will label the topological sectors within the Coulomb phase; in confining phases magnetic charge fluctuates wildly and Φ_i^B is no longer a good quantum number, even approximately.

To summarize, the $U(1)$ spin liquid on a 3-torus has a topological degeneracy characterized by six *integers*, with energies that vanish as

$$\begin{aligned} \mathcal{E} \sim & \mathcal{U}_c \frac{(\Phi_0^E)^2}{L} \left[(n_x^E)^2 + (n_y^E)^2 + (n_z^E)^2 \right] \\ & + \mathcal{K}_c \frac{(\Phi_0^B)^2}{L} \left[(n_x^B)^2 + (n_y^B)^2 + (n_z^B)^2 \right]. \end{aligned} \quad (65)$$

In the RK point effective action \mathcal{U}_c vanishes, so the electric topological sectors have zero energy, with only corrections from irrelevant terms possible.

C. Spin-Spin and Plaquette-Plaquette Correlators

We first consider the two-point S^z correlation function; the transverse part of the spin-spin correlator is not gauge-invariant and vanishes. The mappings of Section II C tell us this is given by the electric field correlator. In the cubic case we use the three-site unit cell containing $\{\mathbf{r}_x, \mathbf{r}_y, \mathbf{r}_z\}$. Because of the orientation convention for the electric field, we have $S_{\mathbf{r}i}^z = \exp(i\mathbf{K}_0 \cdot \mathbf{r}) e_{\mathbf{r}i}$, where $\mathbf{K}_0 = (\pi, \pi, \pi)$ and we take $\mathbf{r} = 0$ in the A sublattice. Therefore the spin correlation function will be shifted from the electric field one by \mathbf{K}_0 in the Brillouin zone. For the pyrochlore we use the unit cell of Section II A containing the four sites (\mathbf{R}, i) , where \mathbf{R} labels the centers of up-pointing tetrahedra (up-pointing diamond sites). In this case $S_{\mathbf{R}i}^z = e_{\mathbf{R}i}$.

We calculate the equal-time correlator $C_{ij}^E(\mathbf{r} - \mathbf{r}') = \langle E_i(\mathbf{r}) E_j(\mathbf{r}') \rangle$ in the gauge-fixed continuum theory, where $E_i = \epsilon_{ijk} \partial_j \Upsilon_k$. We illustrate the calculation with a single component:

$$\begin{aligned} C_{zz}^E(\mathbf{R}) &= \frac{\mathcal{K}_c}{2v_p} \int_{|\mathbf{k}| < \Lambda} \frac{k_x^2 + k_y^2}{k} e^{i\mathbf{k} \cdot \mathbf{R}} \\ &= \frac{\mathcal{K}_c}{2v_p} \int_0^\Lambda \frac{dk k^3}{(2\pi)^3} \int d\Omega' \sin^2 \theta' \exp(ikR \cos \gamma), \end{aligned} \quad (66)$$

where we have imposed the hard momentum cutoff Λ , and γ is the angle between \mathbf{k} and \mathbf{R} . Expanding the exponential in Legendre polynomials of $\cos \gamma$, and using the addition theorem to rewrite these in terms of spherical harmonics, the integral can be done to find:

$$C_{zz}^E(\mathbf{R}) = \frac{\mathcal{K}_c}{\pi^2 v_p R^4} (2 \cos^2 \theta - 1). \quad (67)$$

Here θ is the angle between \mathbf{R} and the z -axis. We have dropped terms oscillating at the cutoff wavevector, which are unphysical artifacts of the hard cutoff. Alternatively, we can use a soft cutoff by inserting $e^{-k/\Lambda}$ in the integrand, integrating over all k -space, taking the limit $R \gg \Lambda^{-1}$ and keeping only the dominant powers of R to recover the same result. In the general case we find:

$$C_{ij}^E(\mathbf{R}) = \frac{\mathcal{K}_c}{\pi^2 v_p R^6} (2R_i R_j - R^2 \delta_{ij}). \quad (68)$$

The striking angular dependence of this correlator is a manifestation of the inherent vectorial structure of the $U(1)$ spin liquid, which comes in turn from the vector fields of $U(1)$ gauge theory. For the pyrochlore model in the $U(1)$ spin liquid phase we have:

$$\langle S_{\mathbf{R}i}^z S_{\mathbf{R}'j}^z \rangle \sim (\mathbf{e}_i)_k (\mathbf{e}_j)_l C_{kl}^E(\mathbf{R} - \mathbf{R}'), \quad (69)$$

where \mathbf{e}_i are unit vectors connecting \mathbf{R} with its nearest-neighbor *diamond* sites. In the cubic case:

$$\langle S_{\mathbf{r}i}^z S_{\mathbf{r}'j}^z \rangle \sim \exp(i\mathbf{K}_0 \cdot (\mathbf{r} - \mathbf{r}')) C_{ij}^E(\mathbf{r} - \mathbf{r}'). \quad (70)$$

In the RK point effective theory, a similar calculation shows that both the radial and angular dependence of the correlator changes. It takes the familiar “dipole” form:

$$\mathcal{C}_{ij}^{E-RK}(\mathbf{R}) = \frac{\mathcal{K}_c m}{8\pi R^5} (3R_i R_j - R^2 \delta_{ij}), \quad (71)$$

falling off as $1/R^3$.

It is also interesting to calculate the correlations of the kinetic energy density. In our ring exchange models this naturally lives on the plaquettes and in the cubic case has the form

$$\varepsilon_{rr'} = \frac{1}{2} (S_1^+ S_2^- S_3^+ S_4^- + h.c.) = \cos b_{rr'}. \quad (72)$$

In the pyrochlore model Eq. (72) looks the same, but with ring exchange on the hexagonal plaquettes as in Eq. (9). Long range order at $\mathbf{k} \neq 0$ in $\langle \varepsilon_{ri} \varepsilon_{r'j} \rangle$ would indicate a plaquette density wave state with broken translation symmetry. To simplify notation we work out the cubic case, where

$$\begin{aligned} \langle \varepsilon_{ri} \varepsilon_{r'j} \rangle &\sim \langle \cos(\tilde{b}_{ri}) \cos(\tilde{b}_{r'j}) \rangle_0 \\ &= \exp(-\tilde{b}^2)_0 \cosh(\langle \tilde{b}_{ri} \tilde{b}_{r'j} \rangle_0). \end{aligned} \quad (73)$$

The prefactor involving $\langle \tilde{b}^2 \rangle_0$ is a nonuniversal constant. At large separation, the second factor can be evaluated in the continuum theory, giving:

$$\langle \varepsilon_{ri} \varepsilon_{r'j} \rangle \sim C \left[1 + (\mathcal{C}_{ij}^B(\mathbf{r} - \mathbf{r}'))^2 + \dots \right]. \quad (74)$$

We can immediately write down the magnetic field correlator by duality, which simply interchanges \mathcal{U}_c and \mathcal{K}_c within the Coulomb phase. Therefore

$$\mathcal{C}_{ij}^B(\mathbf{R}) = \frac{\mathcal{U}_c}{\mathcal{K}_c} \mathcal{C}_{ij}^E(\mathbf{R}), \quad (75)$$

and the kinetic energy density exhibits power-law $1/R^8$ correlations and a nontrivial angular dependence.

The RK point theory does not have this self-duality property, so we need to evaluate another integral to find the magnetic field correlator. Using a hard cutoff, one finds *only* unphysical oscillatory terms. Using the $e^{-k/\Lambda}$ soft cutoff, the result is $\mathcal{C}_{ij}^{B-RK}(\mathbf{R}) \propto 1/\Lambda R^6$. This cutoff-dependence indicates that the angular dependence is probably nonuniversal, since there should be other $1/R^6$ contributions with nontrivial angular factors that have been left out of the continuum theory.

D. Monopole Propagator

In this section we calculate the monopole propagator and verify that it falls off exponentially in space and imaginary time, both in the Coulomb phase and at the RK point. This is one of the key properties of the $U(1)$ spin liquid, since at the transition to any nearby confining phase the monopoles will proliferate and condense.

It is most convenient focus on the equal-time monopole propagator $\langle m_R^\dagger m_{R'} \rangle$, working on the spacetime lattice. For $R \neq R'$, this expectation value *vanishes* taken with respect to \mathcal{S}_{lat}^0 because it creates magnetic charge at two points. To understand the true behavior we need to include magnetic charge fluctuations and add the corrections Eq. (55) to the Gaussian action.

For simplicity, we consider only the restricted set of correction terms:

$$-\delta\mathcal{S} = v_2^\tau \sum_{\tau, r} \cos(2\tilde{\alpha}_{r\tau}) + v_2 \sum_{\tau, \langle rr' \rangle} \cos(\alpha_{rr'}^0) \cos(2\tilde{\alpha}_{rr'}). \quad (76)$$

We want to calculate the propagator in perturbation theory in $\delta\mathcal{S}$:

$$\langle m_R^\dagger m_{R'} \rangle = \frac{1}{Z} \int \exp(i \sum_{\langle rr' \rangle} \mathcal{B}_{rr'} \tilde{\alpha}_{rr'}) \exp(-\mathcal{S}_{lat}^0 - \delta\mathcal{S}), \quad (77)$$

where \mathcal{B} is the classical magnetic field due to a monopole-antimonopole pair at R and R' , respectively. To obtain a nonvanishing contribution, we need to bring down correction terms until the complex exponential has been modified to create no magnetic charges. To lowest order we obtain:

$$\langle m_R^\dagger m_{R'} \rangle \sim v_2^{|\mathbf{R}' - \mathbf{R}|} \left\langle \exp(i \sum_{\langle rr' \rangle} \mathcal{B}_{rr'} \tilde{\alpha}_{rr'}) \prod_{rr'=\mathbf{R}}^{\mathbf{R}'} \cos(2\tilde{\alpha}_{rr'}) \right\rangle_0, \quad (78)$$

where the product of cosines is taken over the shortest path connecting \mathbf{R} and \mathbf{R}' ; for simplicity we restrict our attention to geometries where this is unique, although this is inessential. We have also dropped the background field α^0 , which gives only an overall sign. The gauge-invariant part of the expectation value comes from the term in the product of cosines that threads one magnetic flux quantum from \mathbf{R} to \mathbf{R}' , giving a new magnetic field \mathcal{B}' with zero divergence, and allowing us to express the result as the expectation value of a gauge-invariant operator:

$$\langle m_R^\dagger m_{R'} \rangle \sim \left(\frac{v_2}{2} \right)^{|\mathbf{R} - \mathbf{R}'|} \langle \exp(i \sum_{\langle rr' \rangle} \mathcal{B}'_{rr'} \tilde{\alpha}_{rr'}) \rangle_0. \quad (79)$$

What the perturbation theory has done is exactly to connect the monopole and antimonopole with a Dirac string.

The exponential decay is clear from the prefactor in Eq. (79). To evaluate the corrections to this, we apply the Faddeev-Popov procedure to the functional integral for the gauge-invariant expectation value, and calculate using the photon propagator. We could *not* have done this at the outset since the original operator was not gauge-invariant. It is most convenient to integrate by parts inside the exponential to obtain a result in terms of the classical vector potential and the electric field:

$$\langle \exp(i \sum_{\langle rr' \rangle} \mathcal{A}'_{rr'} \tilde{e}_{rr'}) \rangle_0 = \exp \left(-\frac{1}{2} \sum_{\mathbf{r}, \mathbf{r}', i, j} \mathcal{A}'_{ri} \mathcal{A}'_{r'j} \langle \tilde{e}_{ri} \tilde{e}_{r'j} \rangle_0 \right). \quad (80)$$

The necessary integral is quite difficult to evaluate, so we resort to power-counting to determine the largest possible contribution. Consider a spatial separation of R between monopole and antimonopole. One contribution will come from the region near the pair, giving a factor of R^6 from the integration, R^{-2} from the two vector potential factors, and R^{-4} from the electric field correlator in the Coulomb phase. These factors multiply to give a constant, so we expect that the largest possible contribution to the integral is logarithmic in R , which contributes only a power-law prefactor to the propagator. Other contributions involving regions far away from the pair make subdominant contributions. At the RK point there is an extra power of R from the electric field correlator, and the dominant possible contribution is linear in R and gives a correction to the correlation length.

Finally it is clear from these considerations that the unequal-time propagator is not substantially different, and decays exponentially in space and time.

V. EXACT GROUND STATE WAVEFUNCTION

In this section we return to the microscopic spin models, and use the exact ground state at the Rokhsar-Kivelson point to extract information about the physics nearby. We begin with a discussion of the structure of the wavefunction and some simple properties that can be seen analytically, then proceed to a discussion of the numerical evaluation of several quantities. In addition to various equal time correlation functions, we make use of a remarkable property of RK-type points discovered by Henley³⁵ to approximately evaluate the imaginary-time monopole propagator.

We will consider finite-size cubic and pyrochlore lattices in this section. To fix notation, for the cubic lattice L denotes the number of sites on a side of a periodic system. In the pyrochlore case we take periodic boundary conditions so that \mathbf{R} and $\mathbf{R} + L\mathbf{a}_i$ are identified, and we can think of L as the number of tetrahedra along one periodic direction.

A. General Properties

The RK wavefunction is an equal-weight superposition (with positive coefficients) of all possible dimer coverings consistent with the local dimer constraint. In the spin models the electric field can only take on the values $\pm 1/2$, and it is convenient to visualize dimer coverings as zero-divergence configurations of an electric field that can point only forward or backward on each link. Within the vast superposition there are components of every electric topological sector. Since these are not mixed by the dynamics they should be thought of as degenerate but distinct ground states. The RK point exhibits the electric sectors of $U(1)$ topological order, and as in the

Gaussian RK action they are exactly degenerate even in a finite-size system.

To understand what sector to focus on, it is profitable to consider first-order perturbation theory in $\delta V N_f$ away from the RK point. The first-order shift in the ground state energy is $\delta E = \delta V \langle N_f \rangle$, where $\langle N_f \rangle$ is the average number of flippable plaquettes *in a given sector*. For $\delta V > 0$, sectors with *no* flippable plaquettes, and hence no dynamics, will have the lowest energy, and we reach the usual conclusion that a valence bond crystal obtains on this side of the RK point. For $\delta V < 0$, however, the sector with the greatest average flippability wins out. This is in some sense the most disordered sector, and should have $\Phi_i^E = 0$; several numerical checks support this conclusion. We are interested in $\delta V < 0$, so we focus on the zero-flux sector.

We also wish to consider sectors that violate the zero-divergence constraint and contain spinons. Within each such sector, the lowest energy state is again given by an equal-weight superposition of all electric field configurations consistent with a background charge density specifying the spinon positions. These are exact eigenstates with energy $J_z/2$ times the number of spinons, which in a finite-size system is always even. Consider in particular a sector with two spinons. There is clearly zero energy cost no matter how the spinons are moved around, so the RK point is deconfined and has no Coulomb potential between static electric charges. Again, this is consistent with the effective action Eq. (48).

Finally, we calculate the variational energy of the magnetic topological sectors. In general, we create a classical configuration of the vector potential by acting on the RK ground state with the operator $\mathcal{O} = \exp(i \sum_{\langle \mathbf{r} \mathbf{r}' \rangle} \mathcal{A}_{\mathbf{r} \mathbf{r}'} e_{\mathbf{r} \mathbf{r}'})$, just as for the special case of monopole creation in Eq.(61). Of course we expect only that the resulting state has some overlap with the desired eigenstate of the gauge theory. Denote the RK wavefunction by

$$|\psi_{RK}\rangle = \frac{1}{\sqrt{\mathcal{N}}} \sum_{\{e_{\mathbf{r} \mathbf{i}}\}} |\{e_{\mathbf{r} \mathbf{i}}\}\rangle, \quad (81)$$

where the sum is over all configurations of the electric field in the desired sector and \mathcal{N} is the number of states contributing to the sum. Defining $N_f[\{e\}]$ to be the number of flippable plaquettes in a given configuration, and $P_f[\{e\}, \square]$ to be one if the specified plaquette is flippable and zero otherwise, the variational energy of interest is given by:

$$\begin{aligned} E_{var}[\mathcal{A}] &= \langle \psi_{RK} | \mathcal{O}^\dagger \mathcal{H}_{RK} \mathcal{O} | \psi_{RK} \rangle \quad (82) \\ &= \frac{J_{ring}}{\mathcal{N}} \sum_{\{e\}} \left[N_f[\{e\}] \right. \\ &\quad \left. - \sum_{\square} P_f[\{e\}, \square] \exp(2i \sum_{\mathbf{r} \mathbf{r}' \in \square} \mathcal{A}_{\mathbf{r} \mathbf{r}'} e_{\mathbf{r} \mathbf{r}'}) \right] \\ &= \frac{J_{ring}}{\mathcal{N}} \sum_{\{e\}, \square} P_f[\{e\}, \square] \left[1 - \cos((\text{curl } \mathcal{A})_{\square}) \right]. \end{aligned}$$

Here we use notation appropriate to the cubic model; the generalization to the pyrochlore is obvious.

Specifically, consider the case where \mathcal{O} threads one quantum of magnetic flux through the x -direction in the cubic model. Then $\text{curl } \mathcal{A} = 2\pi/L^2$ for plaquettes in the x -direction and zero otherwise, and

$$E_{\text{var}} = n_f L^3 J_{\text{ring}} (1 - \cos(2\pi/L^2)), \quad (83)$$

where n_f is the average flippability per plaquette. For $L \rightarrow \infty$ this energy goes to zero as $1/L$ as expected, and further gives a rough value for the “magnetic stiffness” at the RK point: $\mathcal{K} \approx n_f J_{\text{ring}}$. Using the numerical methods discussed below, for the cubic model in the zero-flux sector we find $n_f \approx 0.260$. For the pyrochlore a similar calculation shows $\mathcal{K} \approx 2n_f J_{\text{ring}}$; the factor of two arises because the flux passes through two kinds of hexagons. In this case we find numerically $n_f \approx 0.175$.

B. Monte Carlo Algorithms and Ergodicity

Because the RK wavefunction has positive and equal weights, equal-time properties can be evaluated by infinite temperature Monte Carlo for the associated *classical* dimer model. The simplest possible Monte Carlo step is to: 1) Randomly choose a plaquette. 2) If the plaquette is flippable, flip it, otherwise do nothing. As desired, this algorithm preserves the electric flux Φ_i^E . For the measurement of the quantities discussed below, the algorithm was run for as many as 10^{11} Monte Carlo steps at a given system size. In some cases these long runs were necessary to achieve good accuracy because the desired quantity was very small.

It is not clear whether the single ring move algorithm is ergodic within each electric field sector. For $L = 2$ cubic and pyrochlore systems we have performed an exact enumeration of all allowed configurations. In the cubic case the zero-flux sector contains 880 states; 864 of these have flippable plaquettes (with $n_f = 1/3$ on average), and are connected under single ring moves. The other 16 states have no flippable plaquettes. For the pyrochlore model there are 384 zero-flux states connected under single ring moves ($n_f = 1/4$), and 12 zero-flux states with no flippable hexagons. Evidently the single ring move algorithm is not ergodic within the zero-flux sector, but it does not matter if we fail to access states with no flippable plaquettes. In our simulations we generate initial configurations for larger lattices by periodically repeating a state from the flippable part of the $L = 2$ zero-flux sector, so more insidious problems could occur if this sector breaks up into multiple flippable subsectors in larger lattices, each closed under single ring moves.

For an analogous two-dimensional model, it is possible to prove that single ring moves are ergodic in each electric flux sector (see Appendix B). In the absence of a similar result in three dimensions, we have checked some of our results for the cubic model with an algorithm due to Barkema and Newman that we believe is

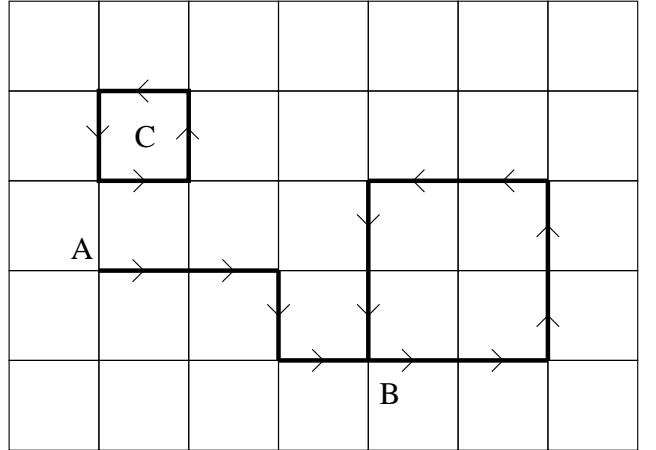


FIG. 7: Illustration of the loop move algorithm of Barkema and Newman looking at one plane of the cubic model. One randomly chooses a starting point (A), and executes a random walk along the lattice bonds, moving only along the direction of the electric field vectors. Once the random walk intersects itself (B), the tail is removed and the electric field is reversed everywhere along the resulting loop, preserving the zero-divergence constraint. If only contractible loops are desired (as in our simulations within the zero-flux sector), one can simply throw away non-contractible loops and repeat these steps until a contractible loop results; this does not affect detailed balance. The single ring move only reverses the electric fields around elementary plaquettes like that at (C).

probably ergodic³⁶. This algorithm is illustrated in Figure 7; in the present case the basic idea is to flip loops of arbitrary length (including single rings), keeping only non-contractible loops that do not change Φ_i^E . All properties measured using both algorithms gave the same results; we present two examples in the following section. While we have not implemented an algorithm with “loop moves” for the pyrochlore model, due to the great similarity of all measured properties to their cubic analogs it seems unlikely that ergodicity is an issue.

C. Equal Time Properties

We measured the electric field-electric field correlator in both the cubic and pyrochlore models. To extract the asymptotic dependence most simply we focused on the correlators measured at a separation of half the system size. It should be noted that one cannot trivially extract the angular dependence discussed in Section IV C by this method, since the two electric field vectors in the correlator will be connected by many paths with length scaling as L but with different angles. For the cubic model we show our results for $\langle e_x(L\mathbf{x}/2)e_x(\mathbf{0}) \rangle$ in Figure 8. Data from both algorithms are shown and the agreement with the $1/R^3$ decay predicted by the effective theory is very good. The same conclusion obtains for the pyrochlore

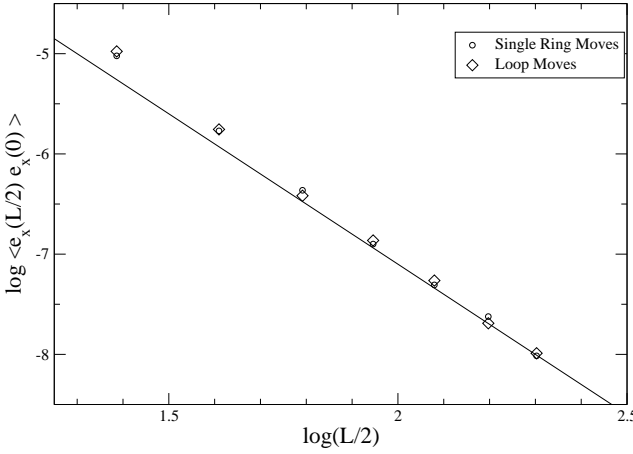


FIG. 8: Log-log plot of the equal time electric field correlator at the RK point of the cubic model, in the orientation discussed in the text. The circles denote data from the single ring move algorithm, while the diamonds were obtained by the loop move algorithm. Error bars are on the order of the symbol size. The line is a guide to the eye with slope -3 to show the very good agreement with the $1/R^3$ decay expected from the effective action.

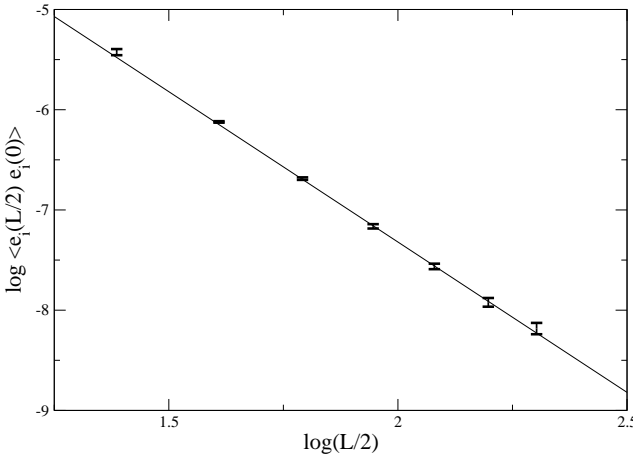


FIG. 9: Log-log plot of the pyrochlore RK point electric field correlator in the orientation discussed in the text. As in Fig. 8, the line is a guide to the eye with slope -3 .

model (but with only the single ring move algorithm). In that case the correlator measured was $\langle e_0(L\mathbf{a}_1/2) e_0(\mathbf{0}) \rangle$; the data are shown in Figure 9. Measurements of other orientations of the electric field correlator in both models all showed the same $1/R^3$ decay.

To measure the equal time monopole propagator it is necessary to address some subtleties that arise when putting objects with gauge charge in a finite-size system. First, it is clear that because the system is a compact manifold with no boundary, it must have zero total mag-

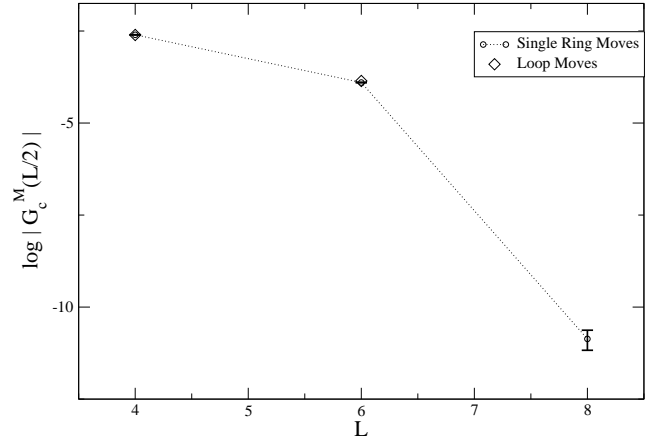


FIG. 10: Cubic model equal-time monopole propagator. The vertical axis is the logarithm of the absolute value of the double-strength propagator discussed in the text, and the horizontal axis is system size. Data for both the single ring move (circles) and loop move (diamonds) algorithms are shown. For the loop move data the error bars are smaller than the symbol size, and for the first two single ring move data points they are obscured by the other symbols. The results are consistent with exponential decay with power-law corrections.

netic charge. Since the operator $m^\dagger(\mathbf{R})m(\mathbf{R}')$ creates a monopole-antimonopole pair, this is not a problem for the propagator. However, consider the cubic lattice and let $\mathbf{R} - \mathbf{R}' = n_x \mathbf{x} \neq 0$. For any value of n_x there will be planes where $\Phi_x^B \neq 2\pi n_x^B$, which is not allowed for a compact vector potential as discussed in Section IV B. We can ameliorate this problem by creating a *double strength* monopole-antimonopole pair, but even in this case the only allowed separation is $n_x = L/2$. Because of these complications, in the cubic case we only measure the double-strength propagator at a separation of half the system size:

$$G_c^M(L/2) = \langle (m^\dagger(\mathbf{R} + L\mathbf{x}/2))^2 (m(\mathbf{R}))^2 \rangle. \quad (84)$$

By time-reversal or Ising symmetry, G_c^M is real. We obtained the vector potential appropriate for Eq. (84) by first solving a discrete Poisson's equation by numerical matrix inversion, then feeding the solution into Eq. (59). This was minimized by a combination of simulated annealing and direct minimization (i.e. zero-temperature simulated annealing). Because of the very rapid decay, it was only practical to measure G_c^M for $L \leq 8$; results are shown in Figure 10 and are consistent with exponential decay with power-law corrections.

On the pyrochlore lattice it is not possible to have double-strength magnetic charges in the microscopic model (see Sec. II E), so for consistency with flux quantization we must consider a more complicated geometry. We look at the following propagator, which creates two monopoles on adjacent up- and down-pointing (dual) diamond sites, and similarly two antimonopoles separated

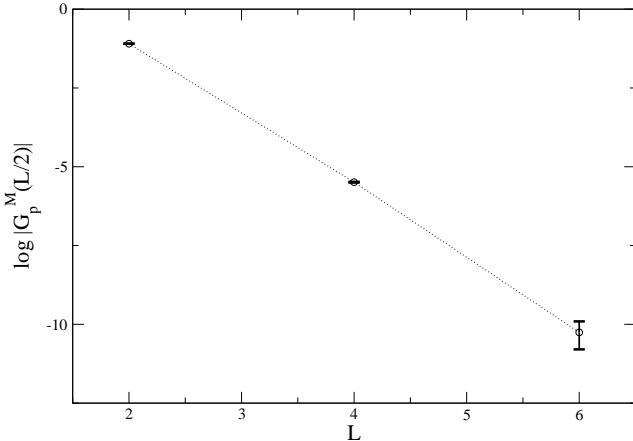


FIG. 11: Pyrochlore equal-time monopole propagator. The vertical axis is the logarithm of the absolute value of the propagator Eq. (85). The results are consistent with exponential decay, with no indication of power-law corrections.

by a distance $L/2$:

$$G_p^M(L/2) = \langle m^\dagger(\mathbf{R} + L\mathbf{a}_0/2)m^\dagger(\mathbf{R}' + L\mathbf{a}_0/2)m(\mathbf{R})m(\mathbf{R}') \rangle, \quad (85)$$

where \mathbf{R} is an up-pointing diamond site and \mathbf{R}' is the down-pointing site directly above. The results are shown in Figure 11, and are consistent with exponential decay; we do not believe the apparent lack of substantial power-law corrections is significant, since the coefficient of these corrections is presumably nonuniversal.

In the cubic model, we also measured the potential between a pair of static spinons in first-order perturbation theory away from the RK point. In the notation of Sec. V A, we consider $\delta V < 0$. The coefficient of $|\delta V|$ in the spinon-spinon potential is given by:

$$V_{\text{spinon}}(\mathbf{R}) = \langle N_f(\text{no spinons}) - N_f(\text{spinons}) \rangle. \quad (86)$$

To measure this quantity, we generated sectors with one $S^z = 1/2$ spinon at $\mathbf{r} = 0$, and another at $\mathbf{r} = (L/2)\mathbf{x} + (L/2 - 1)\mathbf{y}$ for $L \geq 4$. The results are shown in Figure 12, and are consistent with a $1/r$ Coulomb potential. While the perturbation theory does not necessarily “know” whether a deconfining phase with a Coulomb potential can be stable, it does indicate $\mathcal{U}_c > 0$ for small $\delta V < 0$. Since the Coulomb phase *is* stable, we conclude it indeed exists adjacent to the RK point over a finite range $0 > \delta V > \delta V_{\min}$.

D. Monopole Gap

In our models it is possible to approximately measure quantum imaginary time correlation functions using only the classical Monte Carlo dynamics. The key observation, due to Henley³⁵, is that at the RK point the master

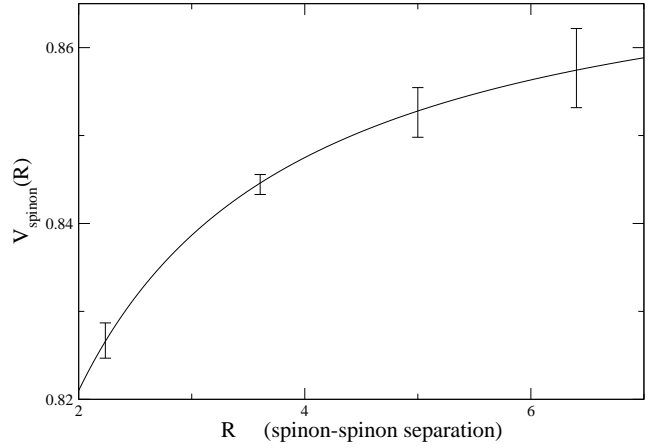


FIG. 12: Plot of the spinon-spinon potential defined in Eq. (86) for several system sizes of the cubic model. The horizontal axis is the distance between the spinons, $R = \sqrt{L^2/2 - L + 1}$. The curve is a fit of the data to the functional form $V_1 + V_2/R$.

equation describing the Monte Carlo dynamics of the single ring move algorithm is *identical* to the imaginary-time Schrödinger equation. We will be interested in monopole correlation functions built from the equal-time correlators constructed above. In the cubic case, for example, we measure:

$$C_c^M(\tau) = \langle \hat{\mathcal{O}}_M \exp(-\tau \mathcal{H}_{RK}) \hat{\mathcal{O}}_M^\dagger \rangle, \quad (87)$$

where $\hat{\mathcal{O}}_M^\dagger = (m^\dagger(\mathbf{R} + L\mathbf{x}/2))^2 (m(\mathbf{R}))^2$. The analogous definition of $C_p^M(\tau)$ for the pyrochlore model is constructed from the equal-time propagator Eq. (85).

To extract information about the spectrum from the simulation, it is useful to relate the units of classical Monte Carlo time to quantum imaginary time. Let N_p be the total number of plaquettes in the system. If we begin with some electric field configuration $\{e\}$ and execute one Monte Carlo step, the probability of remaining in the same state is $(1 - N_f\{e\})/N_p$, while that of making a transition to each of the states accessible by flipping one plaquette is $1/N_p$. We now consider the time-discretized imaginary-time Schrödinger equation and fix the timestep $\Delta\tau$ to recover the same values, which now enter as probability *amplitudes*. We consider:

$$\begin{aligned} & \exp(-\Delta\tau \mathcal{H}_{RK}) |\{e\}\rangle \\ &= \left(1 - \Delta\tau \mathcal{H}_{RK} + \mathcal{O}((\Delta\tau \mathcal{H}_{RK})^2) \right) |\{e\}\rangle \\ &= (1 - J_{\text{ring}} \Delta\tau N_f) |\{e\}\rangle + J_{\text{ring}} \Delta\tau \sum_{\{e'\}} |\{e'\}\rangle, \end{aligned} \quad (88)$$

where the final sum is over those electric field configurations connected to $\{e\}$ by a single ring move. It is only valid to neglect the higher-order terms in $\Delta\tau \mathcal{H}_{RK}$ when $N_f/N_p \ll 1$; in fact, the correspondence between the

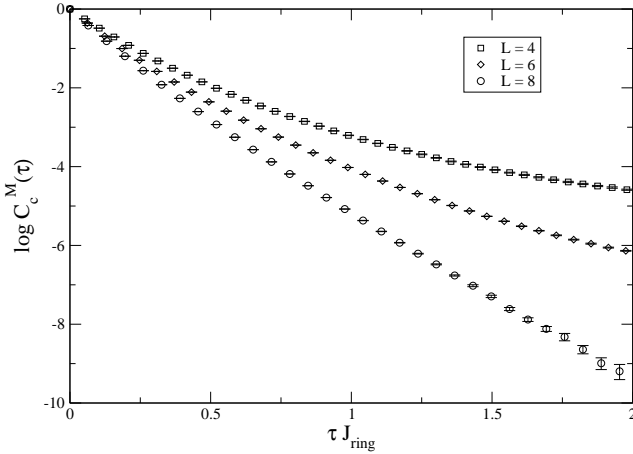


FIG. 13: Logarithmic plot of the approximate monopole-antimonopole imaginary time correlator $C_c^M(\tau)$ for the cubic model. The horizontal axis is imaginary time in units of J_{ring}^{-1} . Data is shown for $L = 4, 6, 8$; as discussed in the text, as L increases the exponential decay in imaginary time becomes cleaner, suggesting the monopole is indeed gapped.

discrete-time quantum dynamics and the Monte Carlo dynamics (which are necessarily discrete in our simulation), is only strictly valid in this limit. In our models N_f/N_p is of order 1/5, so we expect to at best make quantitative errors of about 10%, and at worst to get the wrong answer. This problem cannot be alleviated by the means at hand because the discrete classical algorithm *fixes* the time-step for the quantum dynamics. A more careful treatment would require a direct simulation of the master equation with control over $\Delta\tau$, or quantum Monte Carlo.

If we nevertheless expand the exponential, setting $\Delta\tau = (J_{ring}N_p)^{-1}$ correctly matches the classical probabilities and quantum amplitudes. Using this relation, we write down the appropriate quantity to simulate to measure the imaginary time correlator:

$$C^M(\tau = t/J_{ring}N_p) = \frac{1}{\mathcal{N}} \sum_{\{e\}} \frac{1}{N_{\mathcal{T}(t,\{e\})}} \left[\sum_{\mathcal{T}(t,\{e\})} (\mathcal{O}^M(\{e\}))^* \mathcal{O}^M(\mathcal{T}(t,\{e\})) \right]. \quad (89)$$

Here t is an integer number of steps in Monte Carlo time, and $\mathcal{T}(t,\{e\})$ labels all possible Monte Carlo time evolutions of time t starting from the configuration $\{e\}$. The number of such evolutions is $N_{\mathcal{T}(t,\{e\})}$, and \mathcal{N} is the total number of electric field configurations in the zero-flux sector. Finally, we have defined $\hat{\mathcal{O}}^M|\{e\}\rangle = \mathcal{O}^M(\{e\})|\{e\}\rangle$.

We have measured the monopole imaginary time correlators for both the cubic and pyrochlore models; results are shown in Figures 13 and 14. Note that the extreme long time behavior is not related to the gap; instead, $\hat{\mathcal{O}}^M|\psi_{RK}\rangle$ will have some overlap with the ground

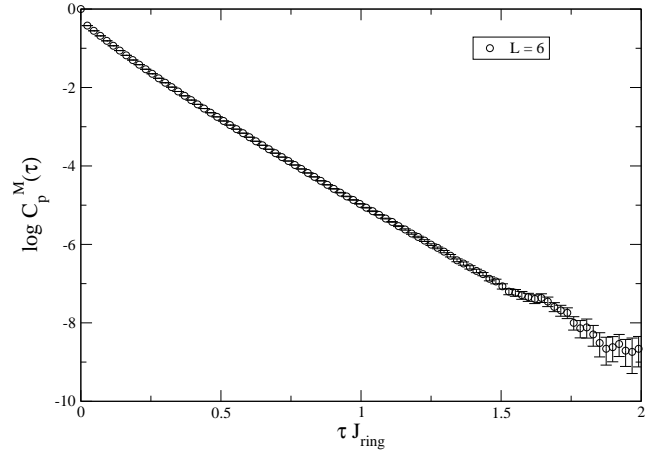


FIG. 14: Logarithmic plot of $C_p^M(\tau)$, the approximate monopole-antimonopole imaginary time correlator in the pyrochlore model. The horizontal axis is imaginary time in units of J_{ring}^{-1} .

state, causing $C^M(\tau)$ to approach a constant as $\tau \rightarrow \infty$. As we go to larger system sizes and the *spatial* separation of the monopole-antimonopole pair in the correlator increases, there is a clean exponential decay persisting for longer times. This is illustrated for several system sizes of the cubic model in Fig. 13. From the numerical data one can extract a rough value for the energy of the monopole-antimonopole configuration put in at $\tau = 0$; in both cases this is about $4.5J_{ring}$. While these results are approximate, it is unlikely that the monopoles are somehow gapless given the circumstantial evidence for a gap, particularly the very rapid exponential decay of the equal-time propagator.

VI. DISCUSSION

In this paper we have argued for the existence of a novel fractionalized quantum disordered state, the $U(1)$ spin liquid, in spin models with a global $U(1)$ symmetry. While we found it necessary to add an extra interaction to the easy-axis limit of the pyrochlore Heisenberg model to proceed analytically, we speculate that this may be only a crutch and that the pure easy-axis model is in the $U(1)$ spin liquid phase. Both the pyrochlore and cubic models have no sign problem, so this issue could be resolved by quantum Monte Carlo simulations³⁷. While it would be a remarkable result if the easy-axis pyrochlore Heisenberg antiferromagnet were a $U(1)$ spin liquid, we believe the results in this paper are enough of an “existence proof” that the phase is likely to be present in less tractable but more realistic microscopic models.

The converse problem, of determining the general requirements for a spin model to exhibit an emergent $U(1)$ gauge structure, is of course more challenging. It would

appear that, since monopole excitations are required to enable a transition to a neighboring confined phase, any such gauge theory must be compact, and hence appear *on the lattice*. Thus, unlike emergent global symmetries, which can appear at low energies and long wavelengths, an emergent $U(1)$ gauge structure would appear to admit only a limited degree of spatial coarse-graining. Given the additional need for spin-carrying degrees of freedom, the unit cell of an emergent gauge theory in a pure spin model would appear to necessarily contain more than a single $S = 1/2$ spin. Based on the present examples, which take advantage of the bipartite structure of the cubic and diamond lattices, it is tempting to speculate that the models should contain a natural bipartite sublattice. It is easy to see, however, that the emergent gauge structure in these models is stable to adding arbitrary weak additional multi-spin interactions, including those that break any bipartite symmetries. Further understanding, including the important issue of whether the $U(1)$ spin liquid is possible in a magnet with global $SU(2)$ symmetry, and if yes, of what its properties might be, must await further study.

Certainly, the most interesting issue is whether the $U(1)$ spin liquid can be found in a real material. The simplest signature is the additive T^3 contribution to the specific heat from the photon. Because it is likely to be possible to quantitatively understand the *phonon* specific heat via independent measurements³³, this could provide a relatively clear and simple test for emergent photons. Further theoretical work may be necessary to understand more delicate probes of the photon, like heat current and (possibly) Raman scattering; phonon-“photon” interactions and disorder may play a nontrivial role. While disorder may be important for some experimental properties, we remark that simple arguments demonstrate that disorder does not destabilize the $U(1)$ gauge structure or the gapless photon.

Since topological order can coexist with conventional broken symmetry, spin liquids are not the only good places to look for emergent photons. One can imagine, for example, condensing spin-carrying but gauge-neutral excitations; in our models this would lead to an ordered magnetic state with gapless spin waves and a $U(1)$ gauge structure. Understanding the possibilities for and properties of phases near the $U(1)$ spin liquid is another problem worthy of consideration if contact is to be made with experiment. Very recently, Senthil, Vojta and Sachdev have made the interesting suggestion that $U(1)$ -fractionalization may provide the answer to some of the puzzles of heavy fermion materials³⁸. We leave these intriguing issues aside to remark that $U(1)$ -fractionalized states are a remarkable and novel possibility for the physics of strongly correlated electrons in *three* dimensions, heretofore a relatively unexplored area.

Finally, we note that Huse, Krauth, Moessner and Sondhi are considering a model closely related to ours³⁹.

Acknowledgments

We thank C. Broholm, C. L. Henley, R. G. Melko, R. Moessner, O. I. Motrunich, R. D. Sedgewick, T. Senthil and A. Vishwanath for numerous stimulating and helpful discussions. M.H. is grateful for support from the Department of Defense through the NDSEG program, and from UC Santa Barbara. M.P.A.F. was generously supported by the NSF under grants DMR-0210790 and PHY-9907949. L.B. was supported by the NSF through grant DMR-9985255, and by the Sloan and Packard foundations.

APPENDIX A: ENUMERATION OF SYMMETRIES

We here enumerate the action of the various symmetries of the cubic model on all the microscopic operators, both in dual and original variables.

- Discrete translations: $\mathbf{r} \rightarrow \mathbf{r} + \mathbf{R}$. The electric field transforms as $e_{\mathbf{r}i} \rightarrow e_{\mathbf{r}+\mathbf{R},i}$, with similar expressions for b and a . Because of the non-translation-invariant background α^0 , the dual vector potential obeys the more complicated transformation law:

$$\alpha_{\mathbf{r}i} \rightarrow \alpha_{\mathbf{R}+\mathbf{r},i} + \delta\alpha_{\mathbf{R}+\mathbf{r},i}, \quad (A1)$$

where the shift $\delta\alpha$ is defined to satisfy

$$\frac{1}{\pi}(\text{curl } \delta\alpha)_{\mathbf{r}+\mathbf{R},i} = e_{\mathbf{r}+\mathbf{R},i}^0 - e_{\mathbf{r}i}^0. \quad (A2)$$

- Lattice rotations: Let \mathcal{R} rotate the lattice into itself about some fixed origin. For example, take the origin to be $\mathbf{r} = 0$ and make a $\pi/2$ -rotation about the z -axis. Then $\mathcal{R}[n_x\mathbf{x} + n_y\mathbf{y} + n_z\mathbf{z}, x] = [-n_y\mathbf{x} + n_x\mathbf{y} + n_z\mathbf{z}, y]$, and so on. We have $e_{\mathbf{r}i} \rightarrow e_{\mathcal{R}[\mathbf{r}i]}$, and similarly for b and a . Again $\alpha_{\mathbf{r}i} \rightarrow \alpha_{\mathcal{R}[\mathbf{r}i]} + \delta\alpha_{\mathcal{R}[\mathbf{r}i]}$, with $(\text{curl } \delta\alpha)_{\mathcal{R}[\mathbf{r}i]} = \pi(e_{\mathcal{R}[\mathbf{r}i]}^0 - e_{\mathbf{r}i}^0)$.
- Reflections: Let \mathcal{F} denote reflection about a plane with normal vector \mathbf{x} , \mathbf{y} or \mathbf{z} . For definiteness, choose the plane with normal \mathbf{x} at $x = 0$, then:

$$\begin{aligned} e_{\mathbf{r}x} &\rightarrow e_{\mathcal{F}(\mathbf{r}),-x} = -e_{\mathcal{F}(\mathbf{r})-\mathbf{x},x} \\ e_{\mathbf{r}i} &\rightarrow e_{\mathcal{F}(\mathbf{r}),i}, \end{aligned} \quad (A3)$$

for $i = y, z$. The vector potential obeys a similar transformation law. The magnetic field and dual vector potential are *pseudovectors* and transform under reflections with an additional minus sign. Again, α transforms with an appropriate shift $\delta\alpha$ to compensate for changes in the background under reflections.

- Gauge and dual gauge invariance: Under gauge transformations, $a_{\mathbf{r}\mathbf{r}'} \rightarrow a_{\mathbf{r}\mathbf{r}'} + \chi_{\mathbf{r}'} - \chi_{\mathbf{r}}$, where χ is a

phase defined on the cubic sites. Similarly we have the dual gauge transformations $\alpha_{rr'} \rightarrow \alpha_{rr'} + \lambda_{r'} - \lambda_r$, with $\lambda_r \in \pi\mathbb{Z}$. In the action the dual gauge transformations can be spacetime-dependent, with

$$\begin{aligned}\alpha_{ri}(\tau) &\rightarrow \alpha_{ri}(\tau) + \lambda_{r+\mathbf{e}_i}(\tau) - \lambda_r(\tau) \\ \alpha_{r\tau} &\rightarrow \alpha_{r\tau} + \lambda_r(\tau + \epsilon) - \lambda_r(\tau).\end{aligned}\quad (\text{A4})$$

- Ising (or particle-hole) symmetry: $e \rightarrow -e$, $a \rightarrow -a$ and $b \rightarrow -b$. Also $\alpha \rightarrow \alpha^0 - \alpha$.
- Time reversal: Since spin operators obey $\mathbf{S} \rightarrow -\mathbf{S}$ under time-reversal, we have: $e \rightarrow -e$, $a \rightarrow a + \pi$ and $b \rightarrow b$. For consistency with the electric field transformation law, $\alpha \rightarrow \alpha^0 - \alpha$. In the action the latter relation continues to hold, as long as we also send $\tau \rightarrow -\tau$. Furthermore, the temporal component of the dual vector potential transforms as $\alpha_{r\tau}(\tau) \rightarrow -\alpha_{r\tau}(-\tau - \epsilon)$. Note that the situation here is the reverse of that in real electromagnetism, where \mathbf{B} changes sign under time reversal and \mathbf{E} is invariant.

These symmetries are all present in analogous forms in the diamond lattice gauge theory. There is also an additional global symmetry, which exchanges the two sublattices of up- and down-pointing sites.

APPENDIX B: ERGODICITY OF SINGLE RING MOVES IN A SQUARE LATTICE MODEL

We consider the classical dimer model on the square lattice at infinite temperature, with two dimers touching every site. This is the $d = 2$ analog of the RK point of our cubic model. We work in the electric field language, where $e_{ri} = \pm 1/2$ with $i = x, y$, and $(\text{div } e)_{\mathbf{r}} = 0$. Consider an $L \times L$ system (L even) with periodic boundary conditions: $e_{[\mathbf{r}+L\mathbf{e}_i],j} = e_{\mathbf{r}j}$, where $\mathbf{e}_i = \mathbf{x}, \mathbf{y}$. The zero-flux sector is specified by the condition:

$$\sum_{n_x=0}^{L-1} e_{n_x \mathbf{x}, y} = \sum_{n_y=0}^{L-1} e_{n_y \mathbf{y}, x} = 0. \quad (\text{B1})$$

We will show that any two states in this sector are connected by a sequence of ring exchange moves on single square plaquettes.

The key step is to go to a height representation on the dual lattice with sites at the plaquette centers $\mathbf{r} = \mathbf{r} + (\mathbf{x} + \mathbf{y})/2$. We define:

$$\begin{aligned}h(\mathbf{r} + \mathbf{x}) - h(\mathbf{r}) &= -2e_{[\mathbf{r}+(\mathbf{x}-\mathbf{y})/2],y} \\ h(\mathbf{r} + \mathbf{y}) - h(\mathbf{r}) &= 2e_{[\mathbf{r}+(\mathbf{y}-\mathbf{x})/2],x}\end{aligned}\quad (\text{B2})$$

The content of this definition is that the height increases/decreases by one if we cross a link of the direct lattice with electric field pointing to the right/left. If we fix the value of the height on one site of the dual lattice these definitions determine it uniquely everywhere. The height is well-defined because the electric field has zero divergence, and can consistently be taken to have periodic boundary conditions because we are in the zero-flux sector.

A flippable plaquette has a height either above or below all of its four neighbors, depending on its orientation. Therefore, in a given configuration, the plaquettes with minimum and maximum height will always be flippable, and every configuration has at least two flippable plaquettes. There are also two states with every plaquette flippable; up to overall shifts of the height these have

$$h(n_x \mathbf{x} + n_y \mathbf{y} + (\mathbf{x} + \mathbf{y})/2) = \pm \frac{1}{2}(1 + (-1)^{n_x + n_y}). \quad (\text{B3})$$

These two configurations are connected by single ring moves, since we can flip all the maximum height plaquettes in one to go to the other.

To complete the proof, we label configurations by $\Delta h = h_{\text{max}} - h_{\text{min}}$. This clearly takes on the minimum possible value of unity in only the two maximally flippable states. Suppose we are in some other state with $\Delta h > 1$. Then we can flip plaquettes of maximum height until Δh is reduced by 1. This procedure can be repeated until $\Delta h = 1$ and we reach one of the maximally flippable states. We have thus shown that any two states are connected by a sequence of single ring moves, because the maximally flippable states are connected to all states and to each other.

¹ P. W. Anderson, Mat. Res. Bull. **8**, 153 (1973).

² P. W. Anderson, Science **235**, 1196 (1987).

³ S.-H. Lee, C. Broholm, W. Ratcliff, G. Gasparovic, Q. Huang, T. H. Kim and S.-W. Cheong, Nature **418**, 856 (2002).

⁴ S.-H. Lee, C. Broholm, T. H. Kim, W. Ratcliff and S.-W. Cheong, Phys. Rev. Lett. **84**, 3718 (2000).

⁵ X.-G. Wen and Q. Niu, Phys. Rev. B **41**, 9377 (1990).

⁶ T. Senthil and M. P. A. Fisher, Phys. Rev. B **63**, 134521 (2001).

⁷ R. Moessner and S. L. Sondhi, Phys. Rev. Lett. **86**, 1881 (2001).

⁸ L. Balents, M. P. A. Fisher, and S. M. Girvin, Phys. Rev. B **65**, 224412 (2002).

⁹ O. I. Motrunich and T. Senthil, Phys. Rev. Lett. **89**, 277004 (2002).

¹⁰ T. Senthil and O. I. Motrunich, Phys. Rev. B **66**, 205104 (2002).

¹¹ X.-G. Wen, cond-mat/0210040 (2002).

¹² O. I. Motrunich, Phys. Rev. B **67**, 115108 (2003).

¹³ T. Senthil and M. P. A. Fisher, Phys. Rev. Lett. **86**, 292 (2001).

¹⁴ J. C. Wynn, D. A. Bonn, B. W. Gardner, Y.-J. Lin, R. Liang, W. N. Hardy, J. R. Kirtley and K. A. Moler, Phys. Rev. Lett. **87**, 197002 (2001).

¹⁵ D. A. Bonn, J. C. Wynn, B. W. Gardner, Y.-J. Lin, R. Liang, W. N. Hardy, J. R. Kirtley and K. A. Moler, Nature **414**, 887 (2001).

¹⁶ X.-G. Wen, Phys. Rev. Lett. **88**, 011602 (2002).

¹⁷ A. M. Polyakov, *Gauge Fields and Strings*, (Harwood Academic, New York, 1987).

¹⁸ The presence of such a gauge structure and the possibility of a Coulomb phase has been realized independently by Moessner, for a pyrochlore Ising antiferromagnet in a weak transverse field. (R. Moessner, private communication.)

¹⁹ D. S. Rokhsar and S. A. Kivelson, Phys. Rev. Lett. **61**, 2376 (1988).

²⁰ C. L. Henley, unpublished.

²¹ P. W. Anderson, Phys. Rev. **102**, 1008 (1956).

²² L. Pauling, *The Nature of the Chemical Bond*, (Cornell University Press, Ithaca, 1938).

²³ A. Paramekanti, L. Balents, and M. P. A. Fisher, Phys. Rev. B **66**, 054526 (2002).

²⁴ L. Balents and A. Paramekanti, Phys. Rev. B **67**, 134427 (2003).

²⁵ E. Fradkin and S. Kivelson, Mod. Phys. Lett. B **4**, 225 (1990).

²⁶ N. Read and S. Sachdev, Phys. Rev. Lett. **62**, 1694 (1989).

²⁷ N. Read and S. Sachdev, Phys. Rev. B **42**, 4568 (1990).

²⁸ J. B. Kogut, Rev. Mod. Phys. **51**, 659 (1979).

²⁹ L. D. Faddeev and V. N. Popov, Phys. Lett. B **25**, 29 (1967).

³⁰ M. Hermele, unpublished (2003).

³¹ A. S. Goldhaber, Phys. Rev. Lett. **36**, 1122 (1976).

³² M. Levin and X.-G. Wen, Phys. Rev. B **67**, 245316 (2003), and references therein.

³³ C. Broholm, private communication.

³⁴ These sectors are known, albeit in a different language, in the context of the pyrochlore Ising model (R. Moessner, private communication).

³⁵ C. L. Henley, J. Stat. Phys. **89**, 483 (1997).

³⁶ G. T. Barkema and M. E. J. Newman, Phys. Rev. E **57**, 1155 (1998).

³⁷ Another point of potential interest in this regard is that the pyrochlore Ising antiferromagnet with a small *ferromagnetic* transverse exchange or small transverse field (see Ref. 18) is likely to have a *U*(1) spin liquid phase; the lowest-order splitting of the low-energy manifold is identical to that in our model. These models have no sign problem and should also be accessible to numerical work.

³⁸ T. Senthil, M. Vojta and S. Sachdev, cond-mat/0305193 (2003).

³⁹ D. A. Huse, W. Krauth, R. Moessner and S. L. Sondhi, cond-mat/0305318 (2003).